

1993

Computer modeling of neutron radiography

Troy J. Groth
Iowa State University

Follow this and additional works at: <https://lib.dr.iastate.edu/rtd>

 Part of the [Mechanical Engineering Commons](#), and the [Nuclear Engineering Commons](#)

Recommended Citation

Groth, Troy J., "Computer modeling of neutron radiography" (1993). *Retrospective Theses and Dissertations*. 232.
<https://lib.dr.iastate.edu/rtd/232>

This Thesis is brought to you for free and open access by the Iowa State University Capstones, Theses and Dissertations at Iowa State University Digital Repository. It has been accepted for inclusion in Retrospective Theses and Dissertations by an authorized administrator of Iowa State University Digital Repository. For more information, please contact digirep@iastate.edu.

Computer modeling of neutron radiography

by

Troy J. Groth

A Thesis Submitted to the
Graduate Faculty in Partial Fulfillment of the
Requirements for the Degree of
MASTER OF SCIENCE

Department: Mechanical Engineering
Major: Nuclear Engineering

Approved:

Signature redacted for
privacy

In Charge of Major Work

Signature redacted for privacy

For the Major Department

Signature redacted for privacy

For the Graduate College

Iowa State University
Ames, Iowa
1993

TABLE OF CONTENTS

ACKNOWLEDGMENT	vii
CHAPTER 1. INTRODUCTION	1
Uses of Measurement Models	3
The Neutron Radiography Measurement Model	7
Monte Carlo Methods	8
Neutron Transport Codes	10
CHAPTER 2. NEUTRON RADIOGRAPHY	14
Requirements	14
Neutron Radiography at Iowa State University	20
Facilities	22
Procedures	24
Uses of Neutron Radiography	25
CHAPTER 3. THE NEUTRON RADIOGRAPHY MODEL	27
Neutron Scattering in Complex Geometries	27
Description of the CAD-interfacing subroutine	30
Determining neutron location	31
Model Components	39
Neutron beam	39

Neutron interactions with matter	40
Indium transfer technique	44
Image production	46
CHAPTER 4. EXECUTION AND RESULTS	48
Program Execution	48
Results	51
Simulation of neutron radiography	51
Validation of program results	56
Effects of scattering	57
Improving execution time	58
CHAPTER 5. CONCLUSIONS	61
Limitations	61
Future Work	62
BIBLIOGRAPHY	65
APPENDIX A. NEUTRON RADIOGRAPHY TERMINOLOGY .	68
APPENDIX B. PROGRAM INPUTS	70

LIST OF TABLES

Table 3.1:	Cross-sections of some common elements and molecules in neutron radiography for 0.0253 eV (2200 m/s) neutrons . . .	44
Table 4.1:	Result of program run on air-conditioner part	56

LIST OF FIGURES

Figure 1.1:	Rotationally symmetric component similar in shape to a jet engine turbine disk	4
Figure 2.1:	2-D model of transfer neutron radiography arrangement . . .	15
Figure 2.2:	Neutron macroscopic cross-sections (1/cm) at 0.0253 eV for various elements. X-ray mass attenuation coefficients (cm ² /g) at 125 keV shown for comparison	18
Figure 2.3:	Neutron microscopic total cross-sections for aluminum and indium	21
Figure 2.4:	Top view of UTR-10 neutron radiography facility	23
Figure 3.1:	Display of parameters returned from CAD-interfacing subroutine for incident neutron and one scattering event	29
Figure 3.2:	I-DEAS CAD model of an auto air-conditioner part depicting triangulation of surface facets	30
Figure 3.3:	Random number distribution showing increased uniformity of distribution for increasing numbers of calls to random number generator	33

Figure 3.4:	Depiction of steps necessary to determine ray path lengths with the CAD-interfacing subroutine. (a) Original sample position. (b) Sample position following shift to place incident neutron path at origin. (c) Inclusion of a scattered neutron path. (d) Shift of scattered path origin to $(0,0,sdist)$	35
Figure 3.5:	Definition of center of mass scattering angles	37
Figure 3.6:	2-D model of neutron radiography simulation	45
Figure 4.1:	Radiograph of the auto air-conditioner part taken with the UTR-10 west beam port	52
Figure 4.2:	Simulated radiograph of the auto air-conditioner part generated with the computer program for $2.0(10^7)$ incident thermal neutrons	54
Figure 4.3:	Sample geometry used for studying effects of undercutting . .	58
Figure 4.4:	Simulation of undercutting by neutrons	59

ACKNOWLEDGMENT

This work was sponsored by the FAA-Center for Aviation Systems Reliability, operated by the Ames Laboratory, USDOE, for the Federal Aviation Administration under Contract No. W-7405-Eng-82 with Iowa State University. The United States government has assigned the DOE Report number IS-T 1626 to this thesis.

CHAPTER 1. INTRODUCTION

The need to examine materials and system components without compromising their integrity has spurred the development of nondestructive evaluation (NDE) techniques. NDE can range from a simple visual inspection of a surface to the measurement of physical properties of materials. The most prominent methods of NDE currently in use include ultrasonic testing, eddy current examination, x-ray radiography, neutron radiography, magnetic flux leakage testing, and liquid penetrant testing [1, 2]. Many of these fields are well developed in terms of their abilities to detect and characterize flaws within a sample.

When nondestructive testing (NDT) was first introduced, the practice consisted of comparison between signals and standards. The standards were generated from a defined set of machined samples incorporated with desired flaws. The testing method was applied to these samples to yield reference signals. Thus when NDT was applied to a component, the resulting signal was compared to the reference signals to determine whether this component was acceptable in a go – no go sense. This type of testing was just a comparison of signals to set points. There was little extraction of the flaw information present in the signal, and the NDT personnel performing the testing often did not understand the physics underlying the generation of the signals.

In comparison, the ability to quantify the signal and understand the causes of

the signal are what sets NDE apart from NDT. In any given inspection, sized flaws with different orientations might produce the same signal. The NDT personnel may not be able to determine the source of the signal. If an inclusion is acceptable in the component while a crack which may produce the same signal is unacceptable, the component will be removed even though it is within standards. However, in NDE one may be able to take the results from the examination and work backwards to determine what produced the signal, thus preventing this type of error. Once an understanding of the physics of signal production is accomplished, a model can be generated which will allow prediction of signals from varying parameters.

Recent advances in the NDE field include the development of measurement models for proving the capabilities of the mentioned NDE techniques for finding and characterizing flaws. The models take parameters controlling the measurement such as ultrasonic frequency, probe diameter, and angle of incidence, and predict the response from the flaw. These models represent a key part of quantitative NDE, i.e., the ability to size and characterize flaws and/or materials. Understanding the details of a process extends the knowledge of what that technique can do. Thus, development of models helps expand the capabilities of the NDE technique. The model inputs should consist of the same parameters varied during an actual inspection. This will allow direct comparison between the results from simulation runs and actual inspections, thus giving a means of validating models. The response of modeled components should be like those of the actual system; not just theoretical or idealized responses based on assumptions which restrict the validity of the model.

Uses of Measurement Models

There are a number of applications and uses of models capable of predicting the signal from an NDE inspection. Models can be applied to inspectability at the design stage of a component, characterization of materials, selection of NDE technique, optimization of NDE parameters, specification of equipment, training of NDE personnel, and development of electronic standards. Other uses of models include the application to plant life extension, and their extension to probability of detection (POD) models.

The first example of the use of these models leads to the incorporation of NDE into the design process. The starting point for NDE in the life cycle of a component occurs in the design process. Models should be used to ensure subsequent inspectability of a manufactured component during both fabrication and service [3]. If the model is exercised on the component design and the POD for the technique is low, two things could be done to improve the POD. Either the component could be modified in the design process so as to maximize the POD, or the inspection technique could be changed to better match the requirements imposed by the design of the component [4].

Models for predicting the POD of flaws are known to exist for the ultrasonic, eddy current, and x-ray techniques. Thompson and Gray have developed an ultrasonic model for relating scattering measurements through liquid-solid interfaces to unbounded medium scattering amplitudes [5]. The modeled ultrasonic testing components included the waves radiated by the probes (for the pitch-catch technique), wave modification by sample geometry, defect effects on wave scattering and propagation, and the effects of signal processing and display. Similar models have been

developed for eddy current examination by Auld *et al.* [6] and for x-ray radiography by Gray [7].

The ultrasonic POD model has been applied to a jet engine turbine disk which is a rotationally symmetric component with a large round head and a slim neck (see Fig. 1.1). At the intersection of the head and neck is a fillet region. With a fillet radius of 0.5 cm and a coarse scan mesh, a cross-sectional display of inspectability shows the POD in the interior of the component near the fillet region to be less than 25%. This low POD was due to the focusing effect of the surface curvature and the depth of the ultrasonic beam focus. Using these results obtained from the model, the scan mesh was refined and fillet radius of curvature was increased to 1 cm. A subsequent exercise of the model following the modifications to scan mesh and radius curvature resulted in a POD greater than 75% in the fillet region [4].

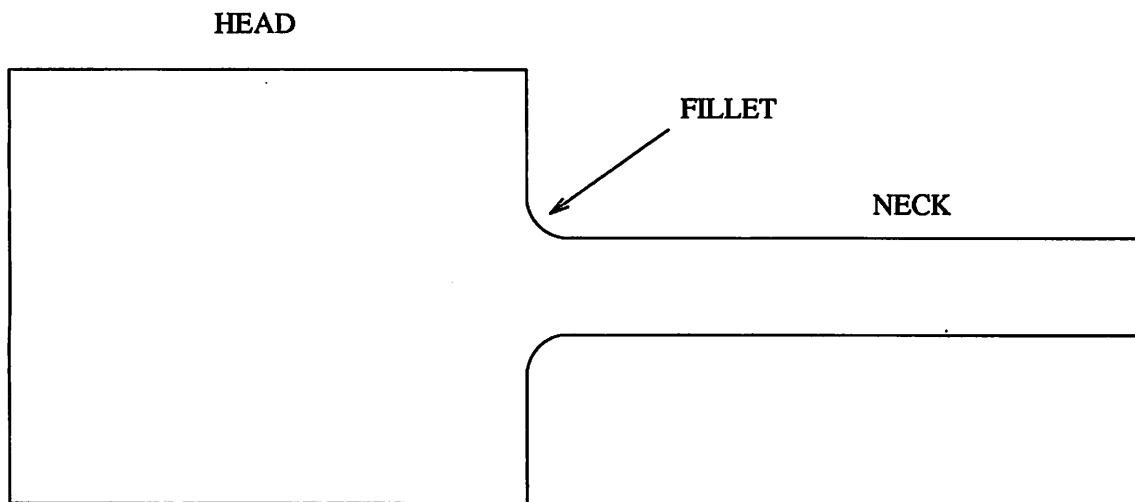


Figure 1.1: Rotationally symmetric component similar in shape to a jet engine turbine disk

Prior to manufacture, procurement of materials and subcomponents must be made. Models of NDE techniques may be used to determine the detectability of variations in material composition. Since the performance of some components is strongly dependent upon their material properties, the need to be able to detect composition variations is readily evident.

During the manufacturing segment and in the in-service phase of a component's life, measurement models may be used for training of NDE personnel. Models are an efficient way to produce a controlled set of signals due to various types and sizes of flaws. These signals can be used to teach the NDE personnel which types of flaws are relevant from a quality control standpoint.

Other uses for models include the choice of optimum inspection technique and, of course, the determination of optimum NDE parameters. There may be several NDE methods which could be applied to a given situation. The model could be used to optimize the various parameters involved in each examination method. Once the best signal for each method is established, each of these signals can be compared in an effort to determine which NDE method is best suited for this inspection need.

Also, the model could be used to determine the inspection capabilities for quality control, or they could be used to determine equipment specifications. The models may be exercised with the parameters and procedures specified by management for quality control. This will determine if these parameters and procedures will have the sensitivity required to detect the desired flaws. In a similar manner, the models can be used to determine the specifications of testing equipment necessary to achieve a desired sensitivity.

Another use for models is the generation of standards for comparison by NDE

personnel with actual signals. This would eliminate the need for production of standard samples with artificially produced flaws. By using a model to produce the signal, better control of the size, type, and location of flaws is obtained.

A measurement model could be used in the field of nuclear power plant life extension (PLEX). As plants approach the end of their design and license lives, the need for reliable methods to inspect plant components magnifies. The first step in using the model for PLEX would be to determine optimal input parameters for actual examination of a component. Second, the model would be used to characterize the minimum detectable size, a , and location of detectable flaws. Then fracture mechanics would be used to predict crack growth rates and the flaw size at which catastrophic failure would occur. If the minimum detectable flaw size is less than the catastrophic failure size, a_c , then NDE should be able to detect flaws before they cause catastrophic failure.

Once a and a_c are established, then a threshold flaw size, a_t , needs to be set. This threshold flaw size is the size above which a component will be retired for cause, and is set at some percentage of a_c . Typically, the NDE parameters are set so that the minimum detectable flaw size, a , is equal to a_t . Thus, all detectable flaws are at or above a_t in size. Examination of the components is then done to look for flaws which exceed a in size. All components meeting this definition are to be taken out of service. Following removal of these flawed components, the largest remaining flaw size is less than a_t . If the rate of crack growth can be determined, the time interval necessary for the size of the largest crack to reach a_t can be calculated. Knowing this time interval allows inspections to be scheduled in a timely manner to ensure against catastrophic failure [8].

The need for measurement models of the more well established NDE techniques, i.e., ultrasonic testing, eddy current examination, and x-ray radiography, is clearly evident from the above discussion. In some instances, however, these methods may prove to be inadequate. In this event, other NDE methods must be investigated. Use of models for economically unattractive methods such as neutron radiography would allow the user of NDE to eliminate the expense of physically setting up an examination merely for the determination of the applicability of such NDE methods. The models may indicate that despite its expense, neutron radiography is the best method available for a particular application. This economic factor is one of the driving forces behind the development of a neutron radiography measurement model.

The Neutron Radiography Measurement Model

A computer code has been written with the objective of modeling neutron radiography; in particular, knowledge of the effects of scattering on the final image was desired. This desire is motivated by the fact that in neutron radiography the scattered component of the beam is the information carrier. The code follows the histories of neutrons in a beam. The user dictates beam characteristics such as flux, location, and cross-sectional area. The initial position of each thermal neutron within the parallel beam is randomly determined. As the thermal neutrons traverse the object of interest, their locations and scattering paths are monitored until the neutron is either absorbed by the material of the sample or scattered out a surface of the sample. Monte Carlo methods are used to model the random behavior of the neutrons as they scatter about the sample.

When a neutron exits the sample in the direction of the converter foil, its in-

tersection point with the foil is calculated. A bin corresponding to this intersection point is then incremented. After all of the histories of the thermal neutrons have been followed, compensation is made for the fast neutron effects on the detection foil and subsequently the radiography film. The program then generates a file which contains the information necessary to produce an image of the simulated radiograph. This density of this image is correlated to the number of neutrons recorded in each converter foil bin. An unique feature of this program is its capability of handling radiography samples with complex geometries. This is accomplished by incorporation of a CAD-interfacing program which allows use of the radiography model on any sample for which a CAD-generated solid model exists.

This program has the possibility for use in more than one application. One area where this code may be used is in the determination of optimal neutron radiography parameters without physically taking a neutron radiograph. The computer code will allow the user to generate simulated radiographs in order to optimize variables such as irradiation time and neutron flux prior to taking an actual neutron radiograph. One or more of the variables could be changed, and then the program could be executed for each different set of parameters. The images produced from these runs would then be compared to determine which set of variables yielded the best image based on contrast comparisons. Once an image of desired quality is generated, the optimum variables are defined.

Monte Carlo Methods

The main focus of this research is the determination of scattering effects of sample geometry on neutron radiography. In order to model the scattering process, Monte

Carlo methods were chosen. The Monte Carlo method is a means of simulating a random process, and although Monte Carlo is a method of statistical trials, it has been applied to problems which have no immediate probabilistic interpretation [9]. The method was developed by Fermi, Ulam, and von Neumann [10] for use in the development of the atomic bomb during the Manhattan Project during World War II. The type of Monte Carlo technique used in this model is a robust method whose results can be used as benchmarks for other more computationally efficient methods.

The fundamental principle of Monte Carlo methods can be explained by an example. First, assume that there are only two types of neutron interactions with aluminum, elastic scattering and absorption. The microscopic absorption cross section for aluminum is 0.23 barns while the microscopic scattering cross section is 1.49 barns. Then under the assumption of only two types of interactions, the microscopic total cross section is 1.72 barns. The ratio of scattering to total cross section is 0.87. To randomly determine which type of interaction will occur, a random number on the interval $0 \leq r < 1$ is generated. If this random number is less than or equal to 0.87 then the interaction type is taken to be a scattering. Random numbers greater than 0.87 indicate absorptions.

Now if 1,000,000 interactions were categorized, one would reasonably expect approximately 870,000 of the interactions would be elastic scattering interactions. Along these same lines, if a large number, N , of random numbers, r , are generated, and these random numbers are uniformly distributed on the interval $0 \leq r < 1$, one would expect approximately

$0.87N$ would fall on the interval $0 \leq r < 0.87$

$0.23N$ would fall on the interval $0.87 \leq r < 1$,

and that the approximation would improve for larger and larger N . Thus, the random number could be used to determine the type of interaction [10, 11]. This method can be extended to continuous probability functions.

Several methods exist for reducing the execution time of Monte Carlo codes while maintaining the statistics. Among the most common of these is biasing with russian roulette. This method is commonly applied in shielding problems. Biasing involves weighting the importance of a neutron. As neutrons traverse an object, many are absorbed or scattered out of the area of interest. However, the neutrons most important to shielding studies are those few which traverse the entire sample. Therefore, a neutron receives higher weighting as it penetrates the material. Also, as the number of neutrons decreases with depth into the sample, splitting, or russian roulette, is performed to maintain a particular neutron flux [9, 10, 12].

Neutron Transport Codes

The idea of using Monte Carlo methods for simulating neutron transport is not new. Many codes have been developed over the years since the Manhattan Project. Usually these codes have a specific application and as such are not universal. However, the basic procedures are similar, and a competent programmer should be able to modify the right code to fit a particular problem. This does not mean that neutron transport codes should be used for modeling neutron radiography. If they could be used for this purpose, they may not produce results of the quality consistent with models designed specifically for neutron radiography. The major limitation inhibiting the simple modification of an existing neutron transport code to perform the desired neutron radiography modeling is the difficulty of geometric modeling encountered in

transport codes.

The general Monte Carlo neutron code MCN was written at the Los Alamos Scientific Laboratory (LASL) by E. D. Cashwell and others. This code uses general three-dimensional geometric configurations to describe the sample. The sample geometry is broken down into any number of cells. First- and second-degree surfaces, as well as some fourth-degree surfaces, form the boundaries for these cells. Examples of first-, second-, and fourth-degree surfaces are a plane, a sphere, and an elliptic torus. Each of the different available surface types are referenced by a specific mnemonic. The location and size of the surfaces are specified by entry of surface equation coefficients in a preset order for each surface.

As stated above, the cells are bounded by surfaces. All the points within a cell must fall on the same side of the bounding surfaces. This requirement prohibits the occurrence of reentrant surfaces. The subdivision of the sample into cells is determined by material interfaces or the restrictions of the bounding surfaces. The number of cells is limited only by the storage capabilities of the computer. The user specifies the material and number density for each cell. Much effort is required of the user in terms of setting up the geometry of the problem. All of the features of the object of interest must be modeled by surfaces such as planes and cylinders, which are very limited in applicability. Small complex features need to be modeled by many such surfaces. Then the user must specify the geographic relationship of the surfaces to one another. All of this geometric modeling requires much time and care from the user.

Once the geometry of the sample has been established, then the paths of the neutrons in the cells can be followed. Standard output of this program includes, but

is not limited to, currents and fluxes across arbitrary surfaces, fluxes at designated points, and average fluxes in designated cells [13, 14]. Because of the complexity involved with specifying the geometry for a given run, MCN is best suited to situations having homogeneous material properties and simple geometries which can be modeled by few surfaces.

A second computer program called NESS (Neutron Elastic Scattering Simulation) was written at the Atomic Energy Research Establishment, Harwell, Berkshire, England for the purpose of Monte Carlo simulation of neutron elastic scattering. The program is divided into four options based upon the type of geometry and the type of cross-section data to be used. The possible geometries are either planar or cylindrical, while the differential cross-section types considered are either monotonic or angularly dependent. The incident beam of neutrons is assumed to be parallel and monoenergetic with even intensity. The program follows the path of each neutron through the sample until the neutron is absorbed or exits the geometry of the sample [11].

Many similarities were found between NESS and the code written here. The general algorithms are very similar. Each starts by calculating how far into the sample the neutron will penetrate prior to interaction. This distance is compared to the straight-line distance through the sample along the incident path. These two distances are compared to determine if the neutron interacts within the sample. The scattering geometry is handled in a similar manner, although NESS utilizes direction cosines to determine the position of subsequent interaction sites. The type of interaction is found in the same way in each program, and this method will be discussed later. Also, both codes can handle nonisotropic scattering.

In contrast to the geometry routines of MCN and NESS, the code developed here uses a triangular-faceted CAD model to describe the surfaces of the sample. This ability to interface with a CAD model is unique in the area of neutron transport or neutron radiography codes. The CAD-interface allows the code to model neutron radiography of any sample geometry provided the user has access to a CAD model of the component. The ability to easily handle neutron scattering in complex geometries is the distinguishing difference between this code and the neutron transport codes, and, in terms of general applicability, is a key feature of the code developed for modeling neutron radiography.

CHAPTER 2. NEUTRON RADIOGRAPHY

Requirements

Standard neutron radiography has four essential components which are illustrated in Figure 2.1. A source of neutrons is needed. This source can be a reactor, an accelerator, a radioisotopic spontaneous neutron source such as californium-252, or an alpha-neutron reaction such as $^{210}\text{Po}\text{-Be}$. Each source has its advantages and disadvantages which must be carefully considered when choosing the appropriate source for an application. The most commonly used neutron source is the reactor due mainly to the high fluxes available when compared to the other types of sources. All of the neutron sources produce fast neutrons.

Fast neutrons are highly penetrating and the cross sections at the fast energy range tend to be small and similar. For these reasons, radiography with fast neutrons is usually avoided. Thermal neutrons are more commonly used in neutron radiography because the neutronic properties of isotopes vary considerably at thermal energies. These variations allow easy detection of material differences within a sample [2]. Since thermal neutrons are used in radiography, the highly energetic neutrons from fission sources must be slowed. Neutron slowing down in a reactor is accomplished by materials such as coolant, moderator, and structural components. However, the beam emanating from the reactor still contains neutrons with a spec-

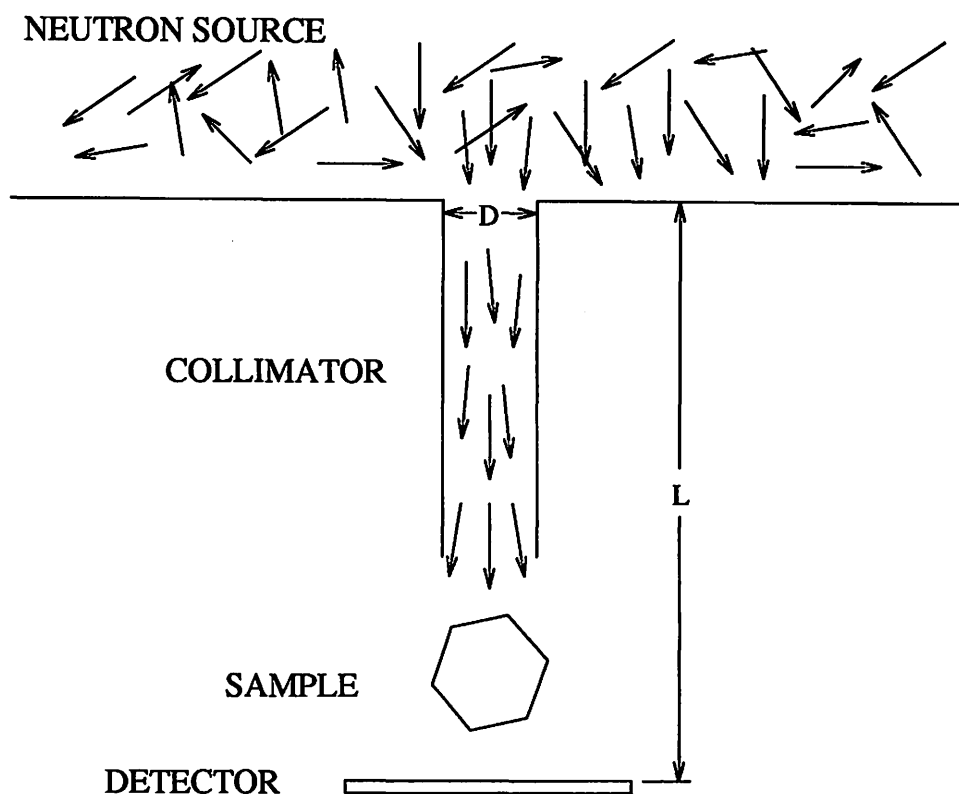


Figure 2.1: 2-D model of transfer neutron radiography arrangement

trum of energies from thermal up to energies on the order of 2 MeV. This leads to the second element required for neutron radiography.

Since the above mentioned neutron sources produce a beam of neutrons of random orientation and direction, a means of collimating the neutrons into a beam is necessary. In effect, collimation removes those neutrons which are not traveling in a desired direction. The need for collimation can be explained with the use of an example. Suppose a bank of lights is used to cast a shadow of an object. The shadow cast will not have defined edges since light from one end of the bank will produce a

shadow of an edge in a different position than will a light from the opposite end of the bank. However, if just one small bright light is used, the edges of the shadow will be more defined. The same holds for neutrons in that a parallel beam yields a much clearer, sharper image.

An important parameter characterizing collimators is the L/D ratio. Fig. 2.1 shows the components of this parameter. The L/D ratio is the ratio of the distance between the inlet aperture and the detector to the inlet diameter of the collimator [2]. Although the L/D ratio is typically used to quantify neutron beams, another important parameter is the actual length of the collimator. A longer collimator will produce a more parallel beam, thus yielding an image with more defined edges. The L/D ratio gives an indication of the effectiveness of the beam, and is sometimes used to compare neutron radiography facilities. A typical value of L/D for a reactor designed to perform neutron radiography should be greater than 100 [15].

The third element of neutron radiography is the composition of the object of interest. An example of the use of neutron radiography is for a part being inspected for hydride corrosion products such as the structure of an aircraft.

Corrosion products are difficult to detect with x-ray radiography. The reason for this difficulty is illustrated in Figure 2.2 which shows the relationship between atomic numbers and X-ray mass attenuation coefficients and neutron macroscopic cross sections. X rays produce a continuous curve. This is because X rays interact with the electrons of an atom. Therefore, materials close together in atomic number have similar X-ray properties and will be difficult to discriminate from one another. Also, the X-ray attenuation coefficient increases with atomic number. Thus, low Z materials will be relatively transparent to X rays. For this reason, X-ray inspection

techniques have limited capabilities for detecting hydride corrosion material. The data for the generation of the X-ray curve in Figure 2.2 was obtained from a personal computer program entitled XCOM [16].

Neutron total cross sections exhibit no relationship with atomic number since neutronic properties are the result of neutron interactions with the nucleus and the properties vary from isotope to isotope. Because of this, materials close to each other in atomic number may be more easily discriminated by neutron radiography than X-ray radiography. Since hydrogen has a relatively high total cross section, it will not allow neutrons to penetrate as easily as aluminum, for example. Therefore, this type of corrosion product will be easier to detect with neutron radiography than with X-ray radiography at the energy depicted in Figure 2.2. Also, since neutron attenuation coefficients are not elemental, neutron radiography can be used for even distinguishing isotopic variations in materials. The neutron macroscopic cross section for hydrogen shown in Figure 2.2 is for unit density hydrogen.

The mean free path, λ , can be used to illustrate the differences between elemental neutron properties. The mean free path is the average distance a neutron will travel between interactions with an atom. The mean free path is calculated from

$$\lambda = \frac{1}{\Sigma_t} , \quad (2.1)$$

where Σ_t is the macroscopic total cross section of the sample material. The macroscopic cross section (cm^{-1}) is the product of the microscopic cross section (cm^2/atom) and the number density of the material (atoms/cm^3). Three consecutive Z elements, iron, cobalt and nickel, have macroscopic total cross sections for 2200 m/s (thermal) neutrons of 1.142 cm^{-1} , 3.948 cm^{-1} , and 1.984 cm^{-1} , respectively [17]. These values when used in Equation 2.1 yield mean free paths of 0.8757 cm, 0.2533 cm, and

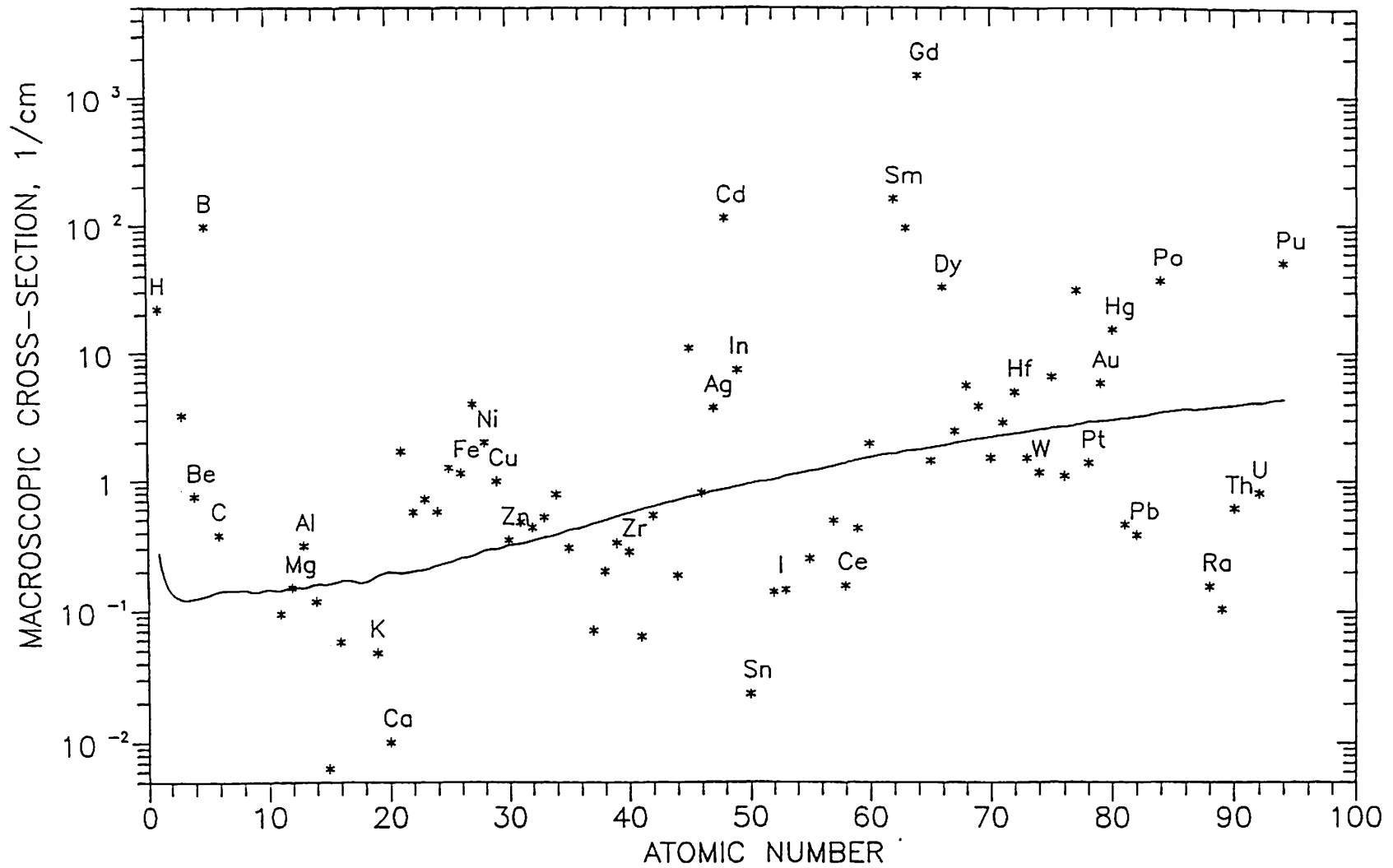


Figure 2.2: Neutron macroscopic cross sections (1/cm) at 0.0253 eV for various elements [17]. X-ray mass attenuation coefficients (cm^2/g) at 125 keV shown for comparison [16]

0.5040 cm for the three elements.

A method of recording the output image is the final component of neutron radiography. Since neutrons are non-ionizing radiation, they will contribute little to the development of radiography film. Therefore, a converter foil is used to produce the ionizing radiation necessary to expose the film. The sample is positioned in the path of the neutron beam. The converter is placed behind the sample and perpendicular to the beam path. The foil absorbs some of the neutrons transmitted by the sample, and then gives off either prompt or delayed radiation, depending upon the material of the foil. There are two different methods for recording this information, the direct method and the indirect or transfer method.

The direct method involves placement of film in the beam between the sample and the converter foil. This is an acceptable method if the sample is not radioactive and the neutron beam is not accompanied by a high flux gamma beam. Typically, the converter material used is gadolinium. The converter foil absorbs the neutrons and promptly emits ionizing radiation such as gamma rays, internal conversion electrons, or alpha or beta particles. The ionizing radiation is then used to record the image on film or track-etch recorders [15].

The indirect or transfer method is commonly used to obtain an image. In this technique, the converter may be a metallic foil such as indium, the actual material of choice is based upon the desired neutronic properties. Those neutrons which pass through the sample activate the converter via neutron capture. In the case of indium, an ^{115}In nucleus absorbs a neutron with the result being the metastable nucleus $^{116}\text{In-m1}$. This reaction takes the form $^{115}\text{In} (n,\gamma) ^{116}\text{In-m1}$. Following irradiation the foil is placed in contact with radiography film. As the $^{116}\text{In-m1}$ isomer decays, the betas

and gammas given off expose the film. Therefore, these forms of radiation expose the film in the same manner an x-ray would.

Figure 2.3 shows the cross-sections for indium and aluminum. The total cross-section for indium drops from 300 b at 0.01 eV to about 90 b at 0.25 eV. From this point it increases sharply to a resonance peak of $3.0(10^5)$ b at 1.45 eV. Several other large resonances occur between 3 and 150 eV. From 150 eV to 1 MeV the cross-section remains relatively constant at a value of about 7 b. In contrast to the erratic behavior of the indium cross-section at relatively low energies, the cross-section for aluminum maintains a value of about 1.5 b from 0.01 eV to 10 keV. Only above 10 keV do resonances occur in the aluminum cross-section. The maximum resonance is only 12 b and takes place at a neutron energy of 0.16 MeV.

Figure 2.3 helps illustrate the differences in neutronic properties of the elements. Since the energy spectrum of a reactor beam is skewed towards the low end, an object made of aluminum will have little effect on the intensity of a neutron beam. However, the higher cross-section for low energy neutrons along with the many resonances of indium will attenuate much of the neutron beam. At higher energies the cross sections for elements tend to be small and similar. Therefore, neither aluminum nor indium will have much effect on the high energy neutrons in the beam.

Neutron Radiography at Iowa State University

Neutron radiography at Iowa State University is accomplished through the use of a beam port on the university's UTR-10 reactor[18]. The UTR-10 is a 10 kW Argonaut-type reactor which is used for teaching and research. The reactor was built in 1959. It is currently powered by plate-type low enriched fuel. The present

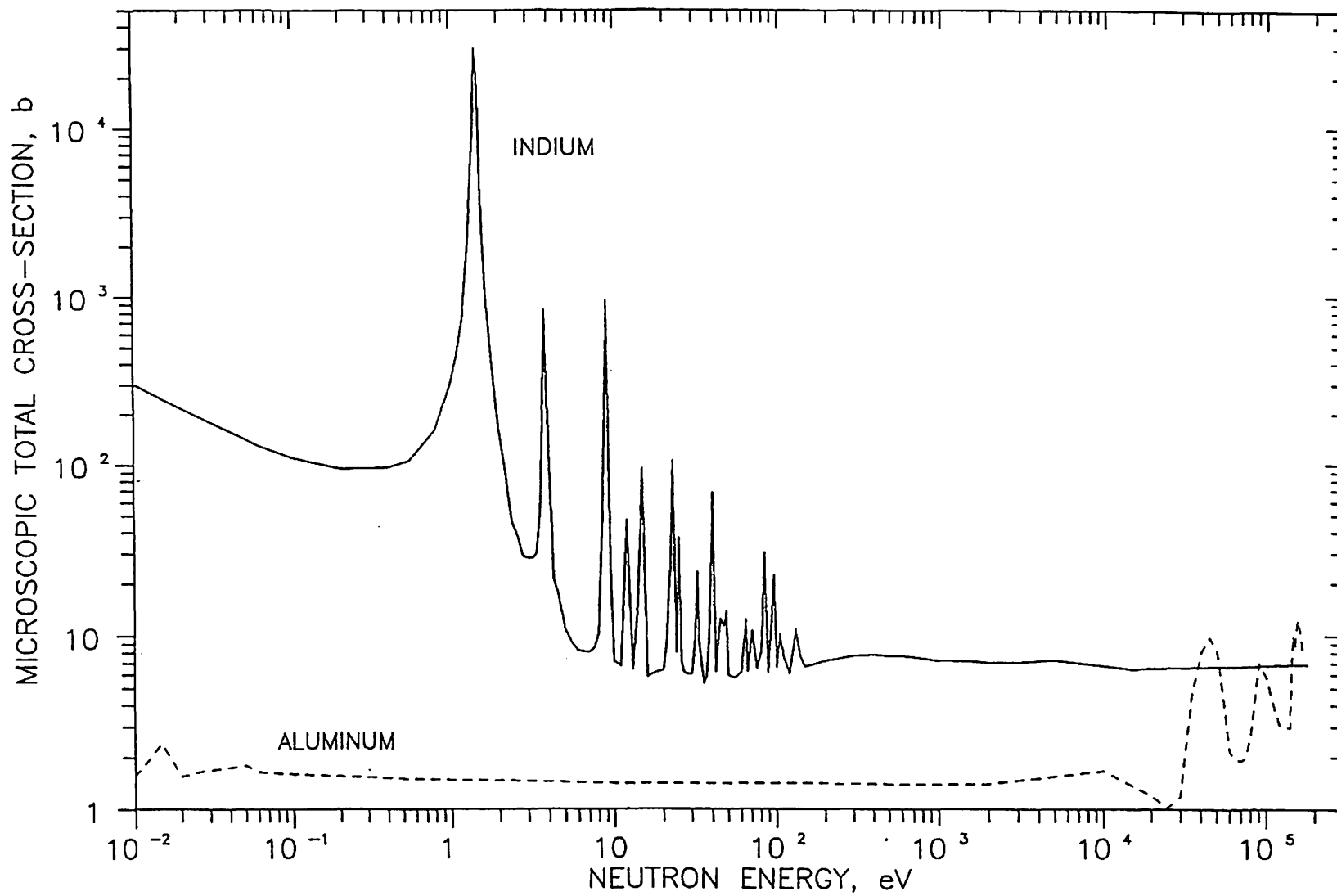


Figure 2.3: Neutron microscopic total cross-sections for aluminum and indium

radiography facility was constructed in 1990. The beam port used is a horizontal port located on the west side of the reactor.

Facilities

The neutron radiography facility consists of a collimator, a sample positioner, a beam stop, and concrete shielding. These components are depicted in Figure 2.4. The collimator is comprised of a lead annulus and a washer-shaped disk of boron carbide which are enclosed by aluminum for structure and protection. The lead annulus is four inches long with an inner diameter of 2.5 inches and an outside diameter of six inches. The boron carbide disk is located on the end of the lead further from the core. This disk is 0.25 inches thick with inner and outer diameters matching those of the lead annulus. The lead serves to reduce the gamma-ray flux of the beam to be collimated, and the boron carbide attenuates undesirable thermal neutrons. Use of the collimator results in a source beam size of 2.5 inches in diameter. Thus, the cross-sectional area of the beam is 32 cm².

The sample positioner is a 4" x 8" x 12" solid cinder block which has been aligned with the beam. The beam stop is made of borated wax which is encased in a wooden box. The paraffin thermalizes the fast neutrons in the beam, and the boron absorbs these neutrons and any thermal neutrons that traversed the sample. The beam stop also minimizes the effects of radiation backscatter of the beam which has passed through the detector. Such backscatter can seriously degrade the quality of an image. The sample positioner and the beam stop are encased within concrete blocks which function as biological shielding. The blocks are of varying sizes, and reduce the dose at the outside of the shielding to 2 mR/hr.

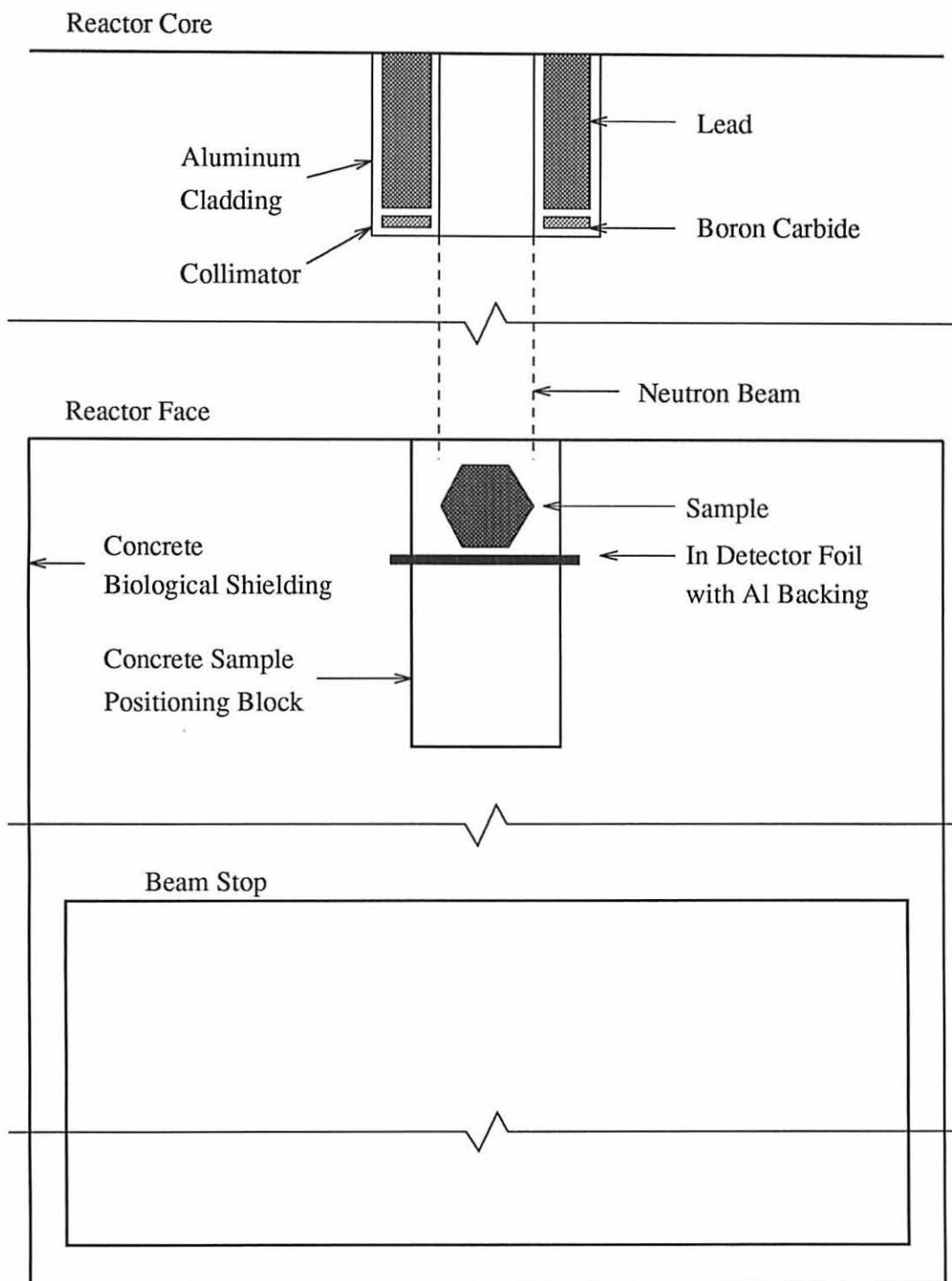


Figure 2.4: Top view of UTR-10 neutron radiography facility

Some of the important characteristics of the beam emanating from this port have been experimentally determined. The thermal neutron flux is $1.3(10^7)$ n/cm²/s, the fast flux is $1.7(10^5)$ n/cm²/s, and the cadmium ratio is 4.8. The cadmium ratio is a measure of the hardness of the neutron beam. This ratio is calculated by dividing the activity resulting from irradiation of a bare gold or indium foil by the activity of a cadmium covered foil of the same material. The L/D was calculated from the geometry of the facility to be 37.6. Experimental measurements determined the L/D to be between 35 and 42 [18].

Procedures

Large concrete shields on top of the radiography facility are removed in order to gain access to the sample positioner. Then the sample is centered on the positioner. The orientation of the sample is dependent upon the features being investigated. Behind the sample is placed the indium foil. Since the thickness of the foil is approximately 0.05 cm, it is taped to an aluminum plate for structural support. After the sample and foil are in place, the concrete shields are replaced.

Then the reactor is brought to the desired power level for the desired irradiation time. Once the irradiation time is reached, the reactor is scrammed. When the reactor power falls below 100 mW, approximately ten minutes after scramming, the radiography facility is opened by removing the top shields. The indium foil is removed under health physics supervision.

The foil is placed in contact with the radiography film and both are covered with lead to reduce the chance of exposure from other radiation sources while the image is being transferred. The lead also serves as a biological shield. The foil and

film are left covered overnight. The half-life of $^{116}\text{In-m1}$ is 54.2 minutes [19] or about one hour. Therefore, after ten hours more than 99.9% of the activated indium has decayed. Leaving the foil and film in contact any longer than overnight will not result in a noticeable difference in the image.

Uses of Neutron Radiography

Neutron radiography has been used to characterize materials quantitatively. Laporte and Mars [20] discuss a method for measurements on the components of a binary alloy. They performed radiography on a platinum/iridium alloy to determine the percent of iridium. A calibration curve was generated by using standard samples of known compositions. All of the samples were machined to a uniform thickness of $1\text{ mm} \pm 10\ \mu\text{m}$. Following radiography of these standard samples, the resulting film densities were plotted as a function of iridium content. Then the curve was used to determine iridium content for unknown compositions based on the film densities from their radiographs. Use of the calibration curve yielded an uncertainty in the iridium content of $\pm 0.25\%$.

Another use of neutron radiography has been for the detection and characterization of flaws. Kedem and Ariel [21] have used neutron radiography to detect silicon inclusions in steel. X-ray or gamma ray methods have been used to indicate the location of large inclusions. However, because of the effect with thickness of the energy spectrum on the attenuation factor, inclusion location and quantification is difficult in thick materials. In contrast, the attenuation coefficient for thermal neutrons experiences little influence from energy changes. Therefore, thermal neutron radiography has proven to be the better technique for obtaining information on inclusions regard-

less of their depth.

Neutron radiography is also performed on reactor fuel rods. Since they are radioactive and emitting neutrons, an external neutron source is not necessary. Also, a radioactive sample would tend to cause exposure of the radiographic film. If x-ray or gamma-ray radiography were used on radioactive objects, some of the information contained in the neutron beam would be masked by film exposure due to the inherent radioactivity of the sample [22].

Measurement models can be used to predict the signals resulting from the above mentioned neutron radiography inspections. Also, a neutron radiography model can be used in the various manners discussed in Chapter 1.

CHAPTER 3. THE NEUTRON RADIOGRAPHY MODEL

The computer code developed for simulation of neutron radiography is comprised of several components. First of all the neutron beam must be modeled. Then a means of handling the complex geometries of a sample and a neutron's path within the object must be addressed. Next, there must be compensation for other factors which affect the radiograph. Finally, there must be a process for generating an image after the lives of the neutrons have been followed.

Neutron Scattering in Complex Geometries

The Monte Carlo technique used in this program could be termed a "brute" force method for following the histories of neutrons. Every random process in nature that is part of a neutron's life in the sample is resolved in a random manner by the program. The neutron's position in the incident beam is determined on a random basis. Also, random numbers are used to determine the scattering angles and the distance between interaction sites. The life of each neutron is followed until it is either absorbed within the sample or leaves the boundaries of the sample. Then the program follows the life of a new neutron.

In order to follow the history of a neutron, the values of several parameters must be known. The neutron's direction must be known. The program must know

where the next interaction site will occur. If the next interaction is a scatter, the angles through which the neutron scatters must be known. Another important piece of information is the distance, ρ , through the sample along the path of the neutron. This is necessary for the determination of whether the neutron remains in the part. This distance is shown in Figure 3.1 along with the entry and exit points, e and f, of a scattered neutron path. The variable d is the distance between interaction sites. Knowing the coordinates of f and of the interaction site, c, allows calculation of the remaining distance in the sample along the current path. If this distance is less than the distance a neutron must travel to the next interaction site, then the neutron will not interact prior to leaving the sample.

The computer code is able to generate a simulated neutron radiograph of any sample as long as the user has access to a CAD model of the sample. Because of the manner in which the information is acquired from the CAD file, the code is currently capable of handling only CAD models generated using I-DEAS , a CAD software package [23]. This commercially available software produces a triangular-faceted solid model of the sample surface. Each triangle is defined by its polygon number and the vertex numbers making up the polygon. Each vertex, or node, in the polygon description of the surface has its own number and (x,y,z) coordinates. Also, the connectivity of the nodes when forming triangles is available. An example of a CAD model of an aluminum casting is shown in Figure 3.2. The triangular facets are readily evident.

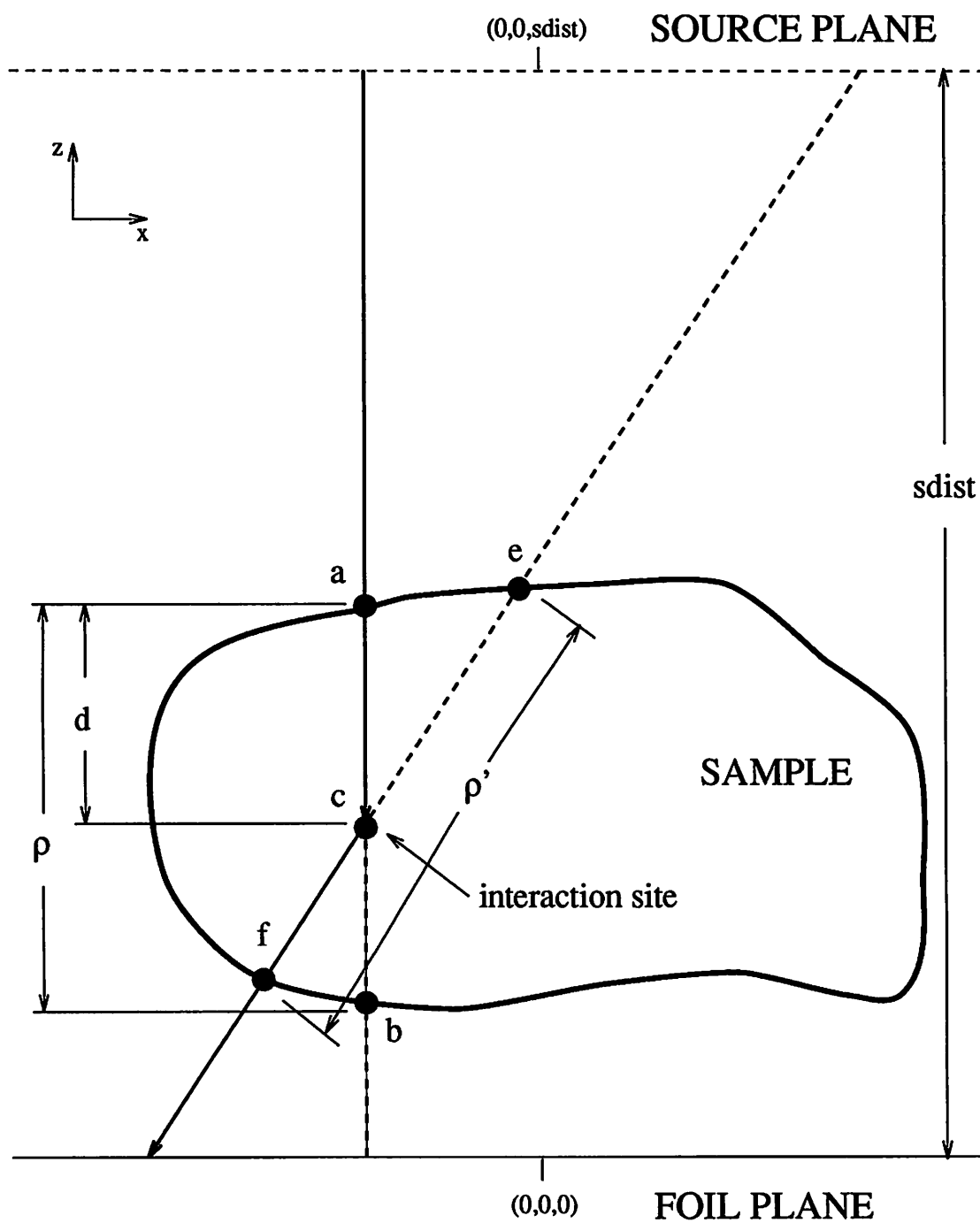


Figure 3.1: Display of parameters returned from CAD-interfacing subroutine for incident neutron and one scattering event

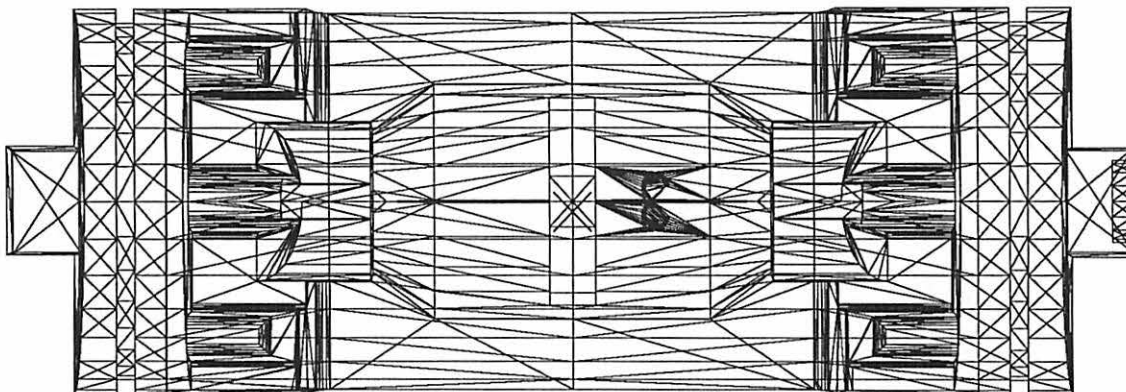


Figure 3.2: I-DEAS CAD model of an auto air-conditioner part depicting triangulation of surface facets

Description of the CAD-interfacing subroutine

When the program reads in the CAD file, each node number and its coordinates are stored in an array. In another array is stored the connectivity information for each polygon. The connectivity information includes which nodes define a polygon and the order of the node numbers. The order is important because it is used to define the normal vector to the polygon. The node order must always be counter-clockwise when viewing the polygon from outside the solid model of the surface. The reading of the CAD file is done only once for each execution of the program.

After the path of the neutron is determined, a perspective transformation is done on the CAD model. This transformation adjusts the coordinates of every node to make the neutron appear to be going in the negative z direction along the z axis. Following the transformation, the normal vectors of the polygons are calculated. All of this information is loaded into another array of size $(n,13)$ where n is the number of polygons. The first nine elements associated with each polygon are the x , y , and

z coordinates of the nodes defining the polygon. The next three elements are for the normal vector to the polygon. The thirteenth element is a tag for later use which indicates whether the neutron path is inward or outward with respect to the sample surface.

The next step taken by the CAD-interface subroutine is to sort the nodes based upon their y coordinates. This results in an array of size (n*3,3) which contains the polygon number, the node number, and the y coordinate of the node. Also out of this procedure comes the maximum and minimum x and y coordinates of the transformed model. Now that the nodes have been sorted, the subroutine determines which polygon edges are intersected by a projection of the neutron's path into the plane $z=0$. The x-intercept values are calculated for any edges which were intersected and these values are sorted. Then, intersected polygons are found along with the z coordinates of the intersection points. After determination of whether the path is in or out of the polygon, the distance between an entry and exit point is calculated for all sets of entry and exit points. Since a path could conceivably exit the sample and then reenter at another point, there may be more than one set of entry and exit points and corresponding path lengths. All of these distances are summed to yield the entire distance of the neutron path within the sample. This distance, ρ , is one of the values returned by the CAD-interfacing subroutine.

Determining neutron location

The key to modeling a neutron's life is answering the question "Is the neutron in the sample?" The CAD-interfacing subroutine is used to find the information necessary to answer this question. The subroutine calculates the distance, ρ , through

the sample on the path of the neutron, and also returns the coordinates of the entry and exit points of the path, $xyzin(x,y,z)$ and $xyzout(x,y,z)$ respectively. In Figure 3.1 points a and b are the entry and exit points of an incident neutron path with the sample. Points e and f are the entry and exit points of a scattered neutron path. For the case of an incident neutron, the parameter d is the distance to the first interaction site.

The distance d is calculated from

$$d = -\frac{\ln(R)}{\Sigma_t}, \quad (3.1)$$

where R is a random number and Σ_t is the macroscopic total cross section of the sample material [11, 12]. The total cross-section is comprised of the absorption and scattering cross-sections. The pseudo-random number generator used in this code produces numbers which are uniformly distributed in the range (0,1] with a period of 2^{32} . All subsequent references to random numbers imply numbers which meet these characteristics. Figure 3.3 shows how well the random number generator performs in terms of distribution uniformity. One million, ten million, and 100 million random numbers were generated for the development of this bar graph. The random numbers were stored in twenty bins of equal width. The first bin contains numbers in the range $0 < R \leq 0.05$, and the last bin contains numbers in the range $0.95 < R \leq 1$. As expected, the percentage of random numbers in each bin is approximately 5%. Also, the uniformity of distribution improves as the number of calls to the random number generator increases.

One of the important features of the CAD-interfacing subroutine to keep in mind is that the path of a particle is assumed to always originate at the point (0,0,*sdist*). The variable *sdist* is a user specified parameter for the perpendicular distance from the

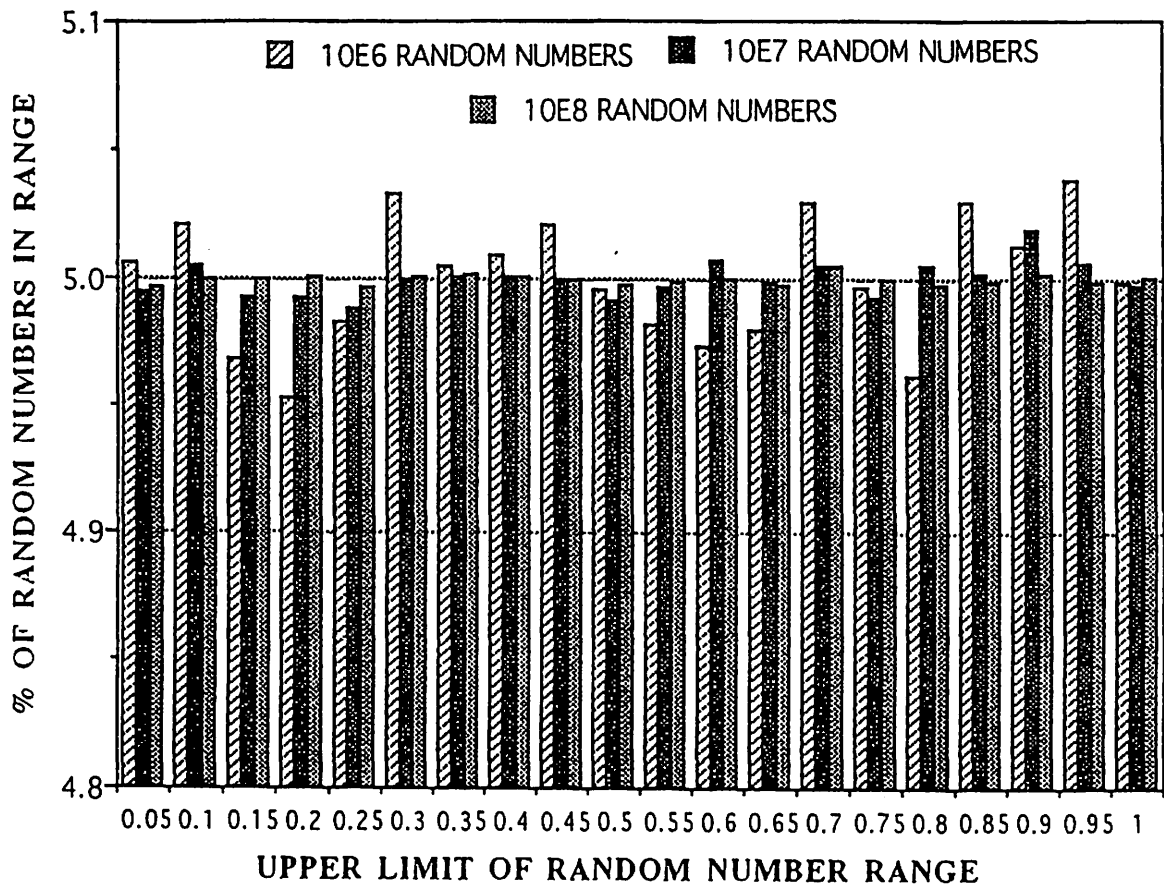


Figure 3.3: Random number distribution showing increased uniformity of distribution for increasing numbers of calls to random number generator

source plane to the foil plane (see Figure 3.1). Also, the CAD-interfacing subroutine is capable of handling ray paths which are not perpendicular to the film plane. In other words, although the ray path must originate at $(0,0,sdist)$, any position $(x,y,0)$ is allowed for the end of the ray path.

The steps necessary to determine ray path lengths are depicted in Figure 3.4. The incident neutron position within the beam is determined randomly in a manner discussed in the section on the neutron beam below. The incident neutron path intersects the foil plane at the point Detect $(X,Y,0)$. Figure 3.4(a) shows the original

position of the sample with respect to the reference lab system origin and the incident neutron location. After the x and y coordinates of the incident neutron are established, the position of the sample is shifted.

The amount of the shift in the x and y directions is equal to the magnitude of Detect(X) and Detect(Y) and opposite in sign. Therefore, if the x position of the incident neutron path is -3 then the sample is shifted by 3 units in the positive x direction. This shift is accomplished by adding the constant 3 to all of the x values for sample node coordinates. The shifted coordinates are stored in a temporary array in order to retain the original sample coordinates. Detect(X,Y,0) is also shifted the same amount as the sample, and thus now coincides with the origin. Figure 3.4(b) shows the result of a shift in the x direction. The neutron now appears to be incident along the z axis. In this way we are able to extend the positions of the neutron source to accommodate the variable source positions generated from incident and scattered neutron paths.

After the sample coordinates have been shifted, the CAD-interfacing subroutine is called. The CAD-interfacing subroutine uses the information acquired from the I-DEAS CAD file to determine which polygons are intersected by a neutron's path. By comparing the geometry of the neutron path with the coordinates of the nodes, the polygons through which the path enters and exits the sample can be determined. Once these polygons are known, geometry establishes the entry and exit points' coordinates as well as the distance through the sample on the path, ρ .

The distance, d, to the interaction site from the entry point is compared to ρ . If d is less than ρ , then the interaction site, c, falls within the sample as in Figure 3.4(b). Otherwise, the neutron passes through the sample without interacting. In this case,

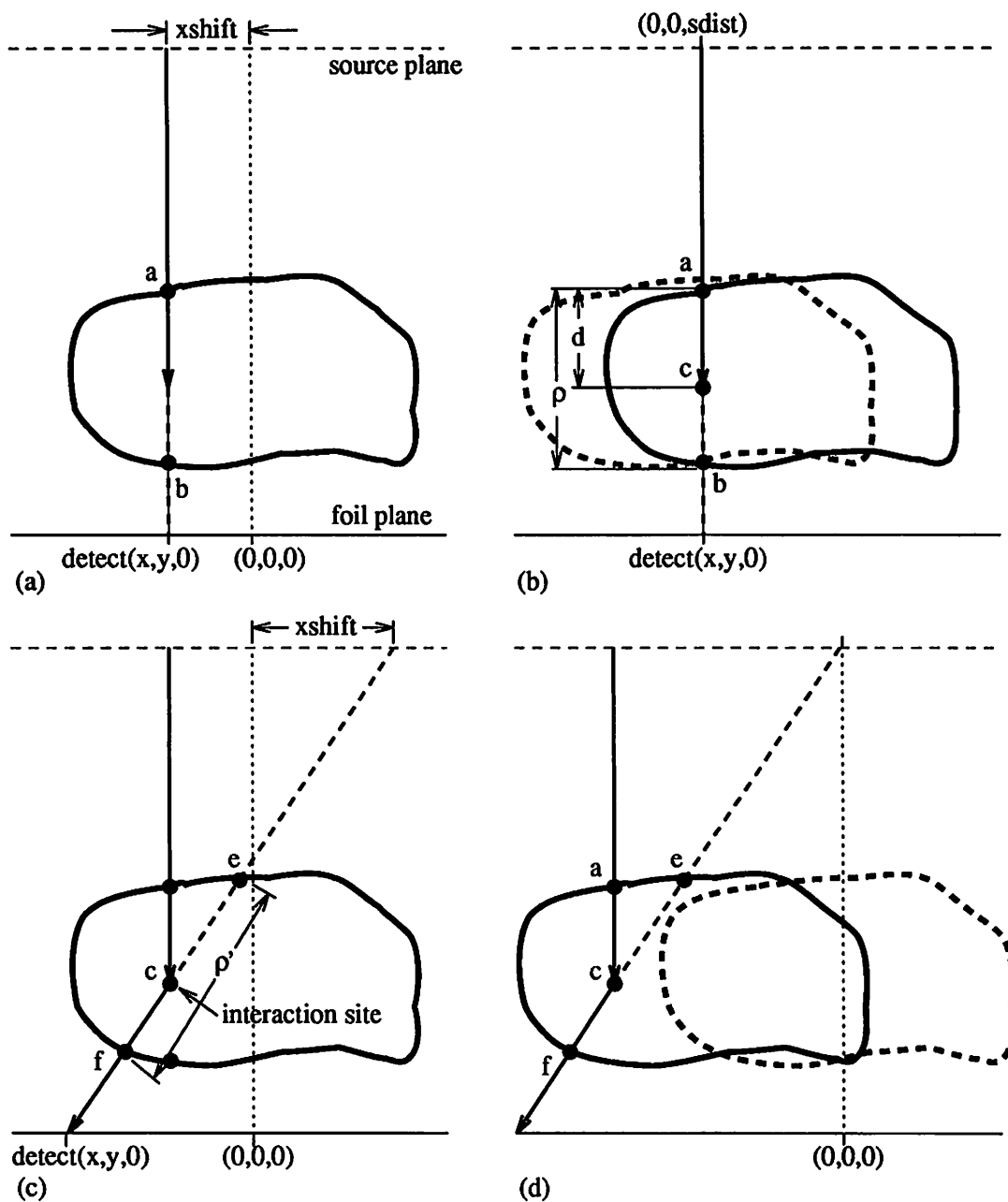


Figure 3.4: Depiction of steps necessary to determine ray path lengths with the CAD-interfacing subroutine. (a) Original sample position. (b) Sample position following shift to place incident neutron path at origin. (c) Inclusion of a scattered neutron path. (d) Shift of scattered path origin to $(0,0,sdist)$

the neutron will be incident upon the foil, and the position of incidence is stored in a bin corresponding to a pixel of finite size. Also, the register containing the number of neutrons incident upon the foil is incremented.

If the interaction site is within the sample, the type of interaction event is determined in the following manner. The ratio of the scattering microscopic cross-section to the sum of the scattering and absorption microscopic cross-sections is calculated. Then a random number, R , is generated. This random number, R , is compared to the cross-section ratio. If R is less than or equal to the ratio then the event is classified as a scattering interaction. In this case the position of the first scattering site is calculated by subtracting the parameter d from the z coordinate of the entry point. The x and y coordinates of the scattering site are equal to those of $\text{Detect}(X,Y,0)$. Otherwise, if R is greater than the cross-section ratio, the event is an absorption [9, 11].

If the previous interaction was determined to be a scatter within the sample, the life of the neutron must still be followed. The sample is returned to its original position by using the original array of node coordinates for subsequent calculations. The next step is to determine the position of the next interaction site. To do this, the distance to the interaction site and the scattering angles must be determined. The angles for neutron scattering are generated randomly in the center of mass (CM) system. The scattering is assumed to be isotropic in the CM system which is a valid approximation for low Z materials. These angles are obtained from a call to the subroutine "Generate". Generate makes three calls to the random number generator. The first will be used to calculate the distance between interaction sites. The second and third calls to the random number generator are used to determine the scattering

angles. Within Generate, the random numbers returned from the second and third calls are modified. The second call is scaled to range in value from 0 - π , while the third is changed to take on values between 0 - 2π . These ranges coincide with the ranges of values possible for the CM angles defined in Figure 3.5.

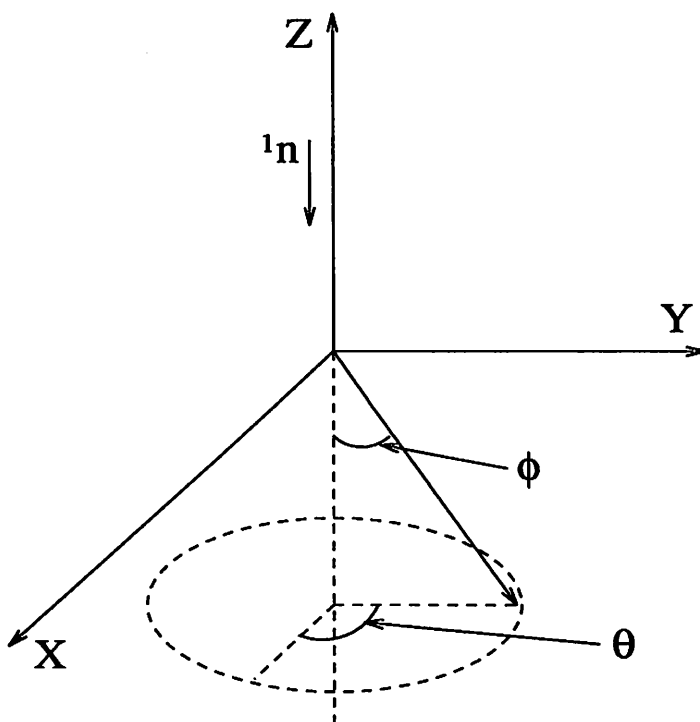


Figure 3.5: Definition of center of mass scattering angles

To convert the scattering angle ϕ to the laboratory system (LAB), Equation 3.2 is used:

$$\phi_L = \arctan \left(\frac{\cos \phi_C}{\sin \phi_C} + \frac{M_n}{M_x} \right) \quad (3.2)$$

where M_n is the mass of a neutron, M_x is the atomic weight of the scattering nuclei, and the subscripts L and C refer to the LAB and CM systems, respectively [24]. It should be noted that the angle θ_C is equal to θ_L , and thus no transformation between

coordinate system is necessary for this angle.

The distance a neutron will travel between interactions is a function of the mean free path for the material. This distance was randomly determined when Generate was called to find the scattering angles. Equation 3.1 was used by this subroutine to calculate d . The distance to next interaction and the scattering angles are relative to a local coordinate system where the current interaction site is the origin and the path from the previous scattering site is taken as the positive z -axis. The coordinates of the next interaction site are calculated in this local system. Once coordinates of the scattering site in the local system are known, they must be transformed to the reference lab system. This is accomplished through the use of an Eulerian angle transformation [25]. A scatter neutron path is shown in Fig 3.4(c). The entry and exit points, e and f , are labeled as well as the distance, ρ , through the sample along the path.

Now that the coordinates of the next interaction site are known, the coordinates for the origination and termination of the scattering path can be determined. Then an x -shift can be calculated for this path, and the sample can be shifted so that the neutron path originates at $(0,0,sdist)$. The CAD-interfacing subroutine is again called to determine the coordinates of points e and f . The distance between points c and f is then compared to the value of d found above. If the path length within the sample is less than the value of d , the neutron will exit the sample without interacting. However, if the path length is greater than d , the neutron interacted within the sample, and the procedure described above is repeated until the neutron either is absorbed or leaves the sample.

Model Components

Neutron beam

As with any model, some assumptions were made during development of this code. Both the fast and thermal neutrons of the incident beam are assumed to be uniformly distributed in the beam. Experimental measurements have shown that there is a slight decrease in the flux near the edges of the UTR-10 beam. However, the majority of the beam has a relatively uniform flux [18]. Also, the epithermal and fast components of the beam are assumed to go straight through the sample without experiencing any collisions. As discussed in the text concerning Fig. 2.3, the cross sections for most materials are relatively low at high neutron energies. Thus, only the lives of the thermal neutrons must be followed in the sample. The total number of thermal neutrons in the incident beam can be found from

$$N = \phi_{Th} t_i A , \quad (3.3)$$

where ϕ_{Th} is the thermal neutron flux, t_i is the time of irradiation, and A is the cross-sectional area of the beam perpendicular to the direction of incident neutron flow. The model assumes the incident thermal beam is monodirectional and monoenergetic. The monoenergetic assumption is valid because the cross-section for many materials of interest such as aluminum, iron, copper, etc. are roughly constant at the thermal energy levels common to nuclear reactor radiography beam. Although only thermal neutrons are followed, a correction is made later for the affects of the fast neutrons on the film. Assuming the beam to be monodirectional implies the L/D is infinity. This is not a very valid assumption for the UTR-10 reactor at Iowa State since the measured L/D ratio for this facility is on the order of 40. However, since most

radiography facilities have an L/D greater than 100, this approximation is acceptable.

In addition to its function described in the section on CM scattering angles, the subroutine Generate is used to define parameters for incident neutrons. Generate makes three calls to the random number generator. The first is used to calculate the distance to interaction site via Equation 3.1. The second and third calls to the random number generator are used to determine the neutron's x-y position in the beam. Within Generate, the random numbers returned from the second and third calls are modified. The second call is scaled to range in value from 0 - π , while the third is changed to take on values between 0 - 2π . The reason for these modifications should be apparent from the discussion on neutron scattering angles. When these values are returned, they are scaled so that the resulting value for neutron x position falls between the minimum and maximum x coordinates of the incident beam and likewise for the y coordinates. The incident beam coordinates are parameters set by the program user and define a rectangular cross-sectioned beam by specification of two points.

Neutron interactions with matter

There are many possible manners in which a neutron can interact with matter. Some of these interactions involve the absorption of a neutron by the nucleus ${}^A_Z X$ resulting in the compound nucleus ${}^{A+1}_Z X$. These compound nuclei have certain nuclear energy levels. If an incident neutron has an energy closely matching the energy of one of the nuclear energy levels, the neutron will have a higher probability of interaction with the nucleus. Such an interaction is termed a resonance reaction. These resonances show up as sharp peaks in the cross-sections at the nuclear energy level.

Examples of such resonance peaks can be seen in Fig. 2.3. All of the different possible reactions of interest in neutron radiography can be classified in two categories: absorption reactions and scattering reactions.

Absorption reactions The absorption reaction category can be divided into many different reactions. In radiative capture, the nucleus absorbs the neutron, a gamma ray is emitted, and a new nuclide is formed having mass number $A + 1$. When a neutron hits a heavy nuclide causing it to split into two medium weight nuclei, fission has occurred. The products of fission include the two new nuclei, some neutrons (usually two or three), and gamma rays. Absorption reactions which are rare in neutron radiography include the (n, α) reaction in which an incident neutron causes the emission of a helium nucleus, and the (n, p) reaction where a neutron is absorbed and a proton is given off. The absorption of neutrons is important in neutron radiography because absorption causes a change in the local flux. Therefore, the presence of different materials can be detected as a result of their cross-sectional influence on the neutron flux. For fissile nuclides such as ^{233}U , ^{235}U , ^{239}Pu , and ^{241}Pu , the dominate absorption mechanism for thermal neutrons is fission. The fission cross-section is two to ten times larger than the radiative capture cross-section for these nuclides. For all other nuclides of interest in neutron radiography, radiative capture is the dominate absorption mechanism.

Scattering reactions In terms of the scattering category, there are three possible reactions. Inelastic scattering occurs when a neutron collides with a nucleus and the neutron imparts some of its energy upon the nuclei before scattering off the nuclei. This energy excites the nucleus to a higher quantum state from which it may

later decay back to its ground state by emission of a gamma ray. Inelastic scattering usually occurs only for relatively high neutron energies because the neutrons must have an energy greater than the energy level of the first quantum state of the nucleus. In other words, there is a fixed amount of neutron energy above which excitation of the nucleus is possible. This threshold energy to the first excited state of a compound nucleus is typically greater than 10 keV, and decreases with increasing Z . As examples, the threshold energy for ^{23}Na is 0.45 MeV and for ^{238}U is 0.045 MeV.

Elastic scattering is the process in which a neutron collides with a nucleus, is absorbed, and then reemitted without leaving the nucleus in an excited state. In contrast to inelastic collisions, kinetic energy is conserved in an elastic scatter, and there is no threshold energy which the neutron must exceed before elastic scattering may take place.

Potential scattering is a common interaction for intermediate energy neutrons. Unlike elastic scattering, in potential scattering the neutron scatters off of the nuclear potential without penetration of the nuclear surface. The cross-section for this interaction is essentially energy-independent and can be approximated by

$$\sigma_p \simeq 4\pi R^2, \quad (3.4)$$

where R , the nuclear radius, is determined from $R \sim 1.25(10^{-13}) A^{1/3}$ cm. For ^{27}Al , the potential scattering cross-section was calculated using Equation 3.4 to be $\sigma_p \sim 1.77$ b. The potential scattering cross-section is relatively constant for neutron energies from about 1 eV to the MeV range.

The type of scattering is dependent upon the mass of the nuclei and the energy of the neutron. In heavy nuclei inelastic scattering is the dominate mode of scattering, while elastic scattering is prominent for lower Z materials. For elastic scattering

in low Z materials, the scattering angle is isotropic in the center of mass system. Inelastic scattering normally occurs for high energy neutrons, while elastic scattering is the mode of prominence for thermal neutrons [24].

Modeled interactions This model allows for two types of neutron interactions with the nuclides of the sample: radiative capture and elastic scattering. Radiative capture is allowed because it is present to some extent in all materials, and it can have a large effect on the flux in materials which have a high cross section for this reaction. Elastic scattering is the only type of scattering event allowed for two reasons. Elastic scattering is the prominent mode of scattering in the neutron energy range of interest, and inelastic scattering can not be modeled without also modeling the energy of the neutrons. For the above reasons and since only thermal neutrons are being modeled, assuming only elastic scattering is a valid assumption. Table 3.1 presents the thermal absorption and scattering cross-sections for some common elements and molecules.

Figure 3.6 shows some of the various processes that may take place in the life of a neutron. A parallel beam of neutrons is shown incident upon a sample of arbitrary shape and material. The letters A through F signify the different events which may take place. Some of the neutrons, A, traverse the part without interacting. Others, B, are absorbed within the part. Still others, C, are scattered by the material, and hit the detector. It is possible for some neutrons, D, to scatter in the direction of the detector but still not hit the detector. Another possibility is that some neutrons, E, will backscatter and exit the sample in the direction opposite the detector. Finally, if the beam cross-section is larger than the sample cross section, some of the neutrons,

Table 3.1: Cross-sections of some common elements and molecules in neutron radiography for 0.0253 eV (2200 m/s) neutrons [17]

element	σ_a , b	σ_s , b
aluminum	0.230	1.49
carbon	0.0034	4.75
hydrogen	0.332	21
iron	2.55	10.9
lead	0.170	11.4
nickel	4.43	17.3
oxygen	0.00027	3.76
titanium	6.1	4.0
uranium	$\sigma_a = 7.59$ $\sigma_f = 4.19$	8.90
water	0.664	103

F, will hit the foil without traversing the sample at all. The difficult part of simulating neutron radiography is following the paths of those neutrons that are scattered.

Indium transfer technique

This portion of the model simulates the transfer method of neutron radiography. In this technique, the sample is positioned in the path of the neutron beam. An indium foil is placed behind the sample and perpendicular to the beam. The neutrons which pass through the sample activate the indium. Both thermal and fast neutrons contribute to the foil activation. Following irradiation the foil is placed in contact with radiography film. As the $^{116}\text{In-m1}$ isomer decays, the betas and gammas given off expose the film. The number of neutrons incident upon the foil is inversely proportional to the thickness of the sample: a thinner sample transmits more neutrons. Thus, the properties of the sample are transferred to the foil and then to the film.

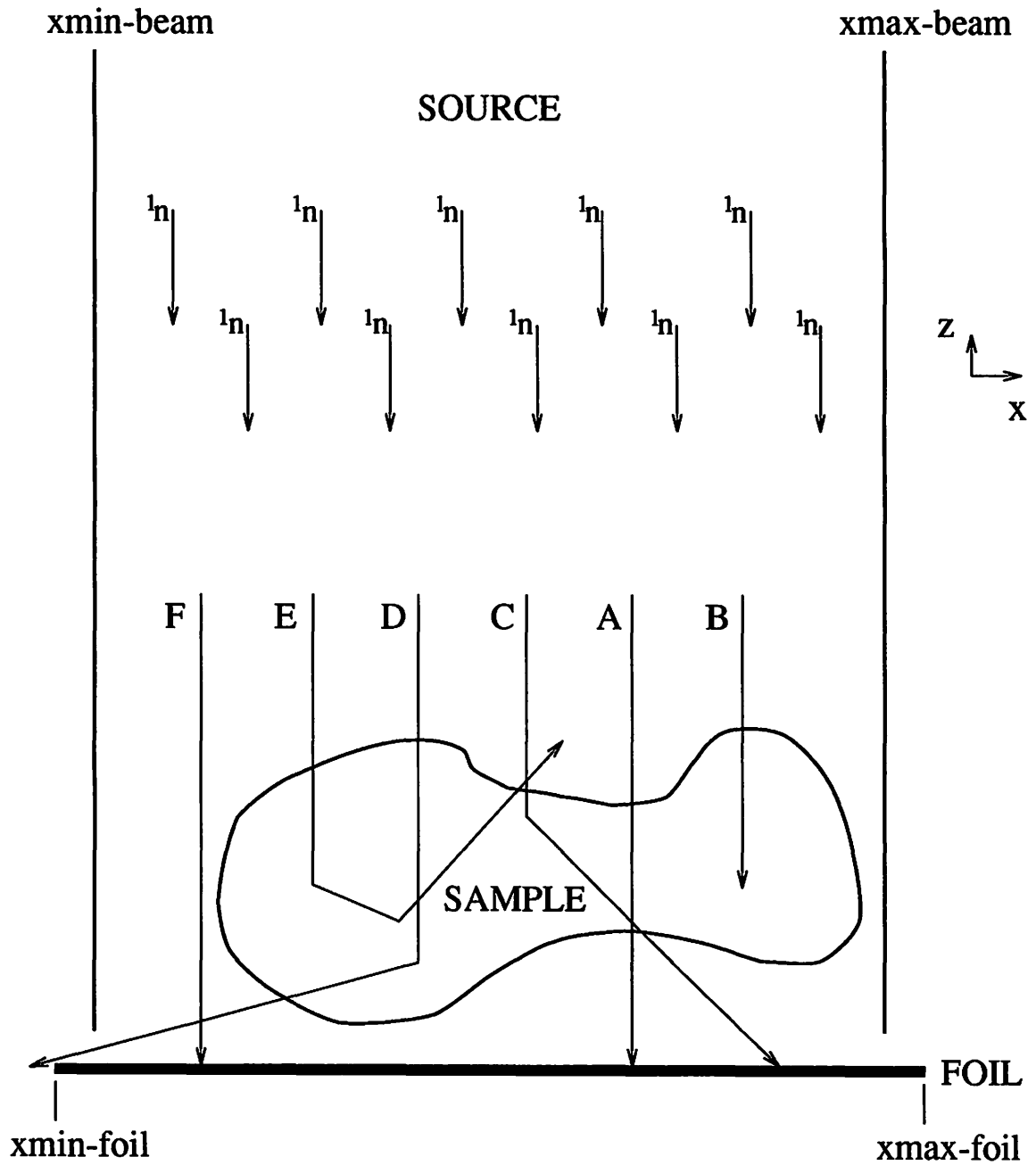


Figure 3.6: 2-D model of neutron radiography simulation

In the case of the simulation, a two-dimensional array serves the function of the foil. The size of the array is established by the user to obtain the desired image sharpness. Usually, a 256x256 array is appropriate. Each array element is congruous to a pixel of an actual radiograph. If a neutron exits the sample and is incident upon the foil, the value of the array element where the neutron's path intersected the foil is incremented by one. In this manner, the number of neutrons that hit each pixel of the foil is recorded.

Image production

Once the program has processed the desired number of thermal neutrons found by Equation 3.3, the information obtained must be converted to an image. The first step in this process is to add a contribution to the foil from the fast neutrons in the beam. Then this result must be adjusted for decay during irradiation, during the time between the end of irradiation and the placement of the foil in contact with the film, and during the time of foil-film contact.

Next, the number and intensity of the betas and gammas emitted from the activated foil must be taken into account. Previous experiments have shown that the betas contribute 85% of the film density for radiographs obtained via the indium transfer method [18]. This contribution is taken into account by converting the number of betas produced from the foil decay to an effective number of gamma rays. These effects have been modeled so that the decay of the activated foil can be used to quantify the development of the film. The final step is to write out a file which contains the information necessary to display an image of the simulated radiograph. The first line of this binary file contains the size of the image, i.e., 256x256. The

remainder of the file contains an array of gray scaled values for each pixel of the image.

The gray scaling of the image can be performed in one of two modes: automatic or manual. In the automatic mode, the array of pixels is searched for the high and low values. Then the cell with the high value is assigned a value of 255, and the cell with the low value is set to 0. All of the other cells are linearly scaled between 0 and 255 based upon their value. In the manual mode, the maximum and minimum cell values about which to scale the image can be specified by the user. If a cell's value is greater than the maximum, it is set to 0. If the value is less than the minimum, it is set to 255. Cells whose values fall between the minimum and maximum are linearly scaled so that their values range from 1 to 254.

CHAPTER 4. EXECUTION AND RESULTS

Program Execution

All runs of the code have been on a DECstation 5000/240 workstation. Some minor modifications to the code would allow for use on other machines. A subroutine has been written which reads an input parameter file. This file has a structured format and contains all the values of the parameters necessary for proper execution. When the program is run, the user is prompted for the name of this parameter file. Instead of having to type the value of every parameter each time the program is executed, the user may simply edit his parameter file. Since there are currently at least 31 different input parameters to the code, the actual number depending on which particular options are chosen, use of such a file has been found to be a great time and labor saver. All of the various parameters are listed and described in Appendix B.

Following the reading of the input parameter file, the execution of the main portion of the program takes place. This is where the lives of the thermal neutrons are simulated and followed. Once the desired number of thermal neutrons has been processed, further calculations are performed to enable generation of an image. There are several outputs following the execution of the program. The array containing the number of thermal neutrons incident on each pixel of the detector foil is written to

a file in ASCII format. This allows the user to further analyze the run. Also output to a file is the number of neutrons which were absorbed, were lost out of the sample in the positive z direction, were lost out of the sample in the negative z direction but at an angle such that they didn't hit the foil, and impacted the foil. And of course, the data necessary to generate an image is written to a file.

There are several factors which have direct bearing on the execution time of the code. These factors include the number of thermal neutrons incident on the sample, the material of the sample, and the complexity of the sample geometry. Obviously, the higher the number of neutrons calculated by Eqn. 3.3, the longer the program takes to complete a run. For runs where the number of thermal neutrons is greater than 1 million, the majority of the execution time is attributable to following the histories of the thermal neutrons. Therefore, for these large runs, execution time is a linear function of the number of incident thermal neutrons.

The number of interactions per unit length is a function of the material mean free path; thus, the type of material effects the execution time. A sample made of aluminum will result in a much faster code execution than a sample made of a hydrogenous material such as wax. Wax has a much shorter mean free path, and thus the number of interactions per path length will be much higher in comparison with aluminum.

The variable which has the greatest impact upon execution time is the CAD file. The air-conditioner CAD file shown in Fig. 3.2 contains 1450 nodes and 2896 polygons. In contrast, a simple rectangular parallelepiped would contain only eight nodes and twelve polygons. Since each neutron interaction requires transforming and sorting the coordinates of the nodes, large CAD files require longer execution

times. Running on a DEC-5000/240 the program took approximately two weeks clock time to generate an image of the air-conditioner sample (Fig. 3.2) using 20 million incident thermal neutrons. For comparison, a rectangular parallelepiped with all the same variables other than the CAD file ran in less than two hours clock time.

In order to improve the execution time of the code, an approximation is made to the method of determining ρ for incident neutrons. Prior to execution, the cross-section of the neutron beam is divided into 256x256 grid elements. Then the values of ρ for perpendicular neutron paths originating at the center of each grid element are calculated. These values and the z coordinates of the path entry points are stored in arrays. Once an incident neutron's position in the beam is randomly calculated, the beam grid element which that position falls within is determined. Then the ρ and z coordinate for this incident neutron path are obtained from the arrays. Thus, all incident neutron positions within a given grid element are assumed to have the same values for ρ and the z coordinate of the entry point.

Prior to incorporation of this approximation, the CAD-interfacing subroutine was called for each incident neutron. Now the CAD-interfacing subroutine is called a total of 65,536, i.e., 256x256, times for all of the incident neutrons. The savings in computation time is readily evident for simulations with millions of incident neutrons.

The above assumption has been shown to be valid for the aluminum casting of Fig. 3.2. A file was generated from the array of ρ values. An image displayed from this file showed sufficient detail of the sample to warrant use of this method. However, if the detail would have been insufficient, two methods could be performed to improve the detail. Either the number of grid elements could have been increased or the cross-sectional area of the beam could have been decreased. The arrays of ρ values

and z coordinates are also stored to an external file. This allows the user to access these arrays for subsequent runs on the same sample in which the beam and sample location are unchanged. This option further decreases the execution time since the arrays are simply read from the external file instead of having to be generated for each similar run.

Results

Simulation of neutron radiography

The code has been used to generate files for image display of various samples including the auto air-conditioner part shown in Figure 3.2. Figure 4.1 is an example of an actual neutron radiograph. The sample was irradiated for two hours at a power of 10 kW. As mentioned in Chapter 2, the thermal flux of the beam is $1.3(10^7)$ n/cm²/s. Thus, use of Eqn. 3.3 yields a value of $3.0(10^{12})$ for the number of thermal neutrons incident upon the sample during irradiation. The actual number of thermal neutrons incident was slightly higher due to those present during the time it took to take the reactor from a cold startup to full power and from full power to shutdown.

Figure 4.2 is a computer simulated radiograph of the same part. The number of thermal neutrons used in the generation of this image was $2.0(10^7)$ which corresponds to a thermal flux of 38.6 n/cm²/s for an irradiation time of 7200 s with a beam cross-sectional area of 72 cm². The gray scaling was done in the automatic mode discussed in Chapter 3. Table 4.1 presents the output from the run used to generate Figure 4.2. The values in this table don't total to $2.0(10^7)$ due to roundoff.

Figure 4.1: Radiograph of the auto air-conditioner part taken with the UTR-10 west beam port

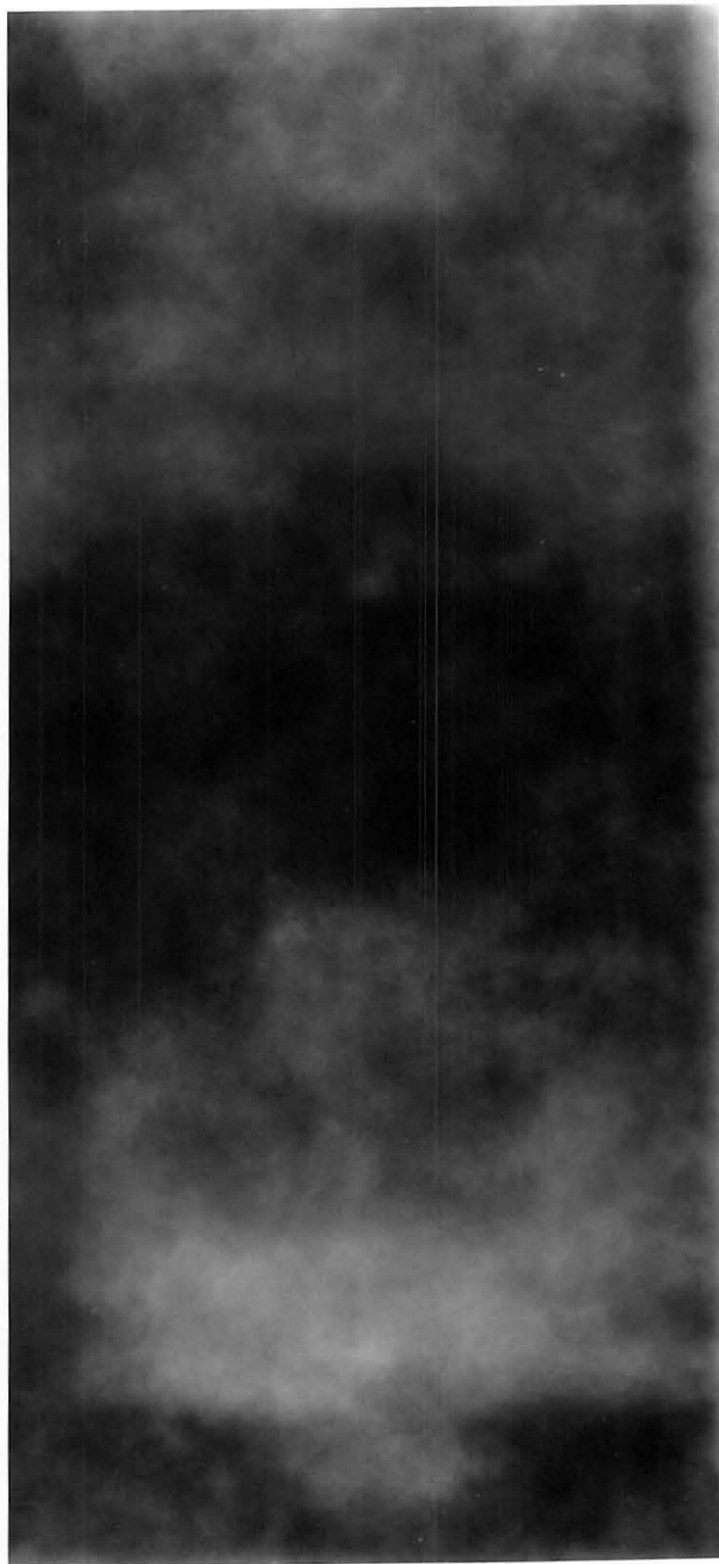


Figure 4.2: Simulated radiograph of the auto air-conditioner part generated with the computer program for $2.0(10^7)$ incident thermal neutrons

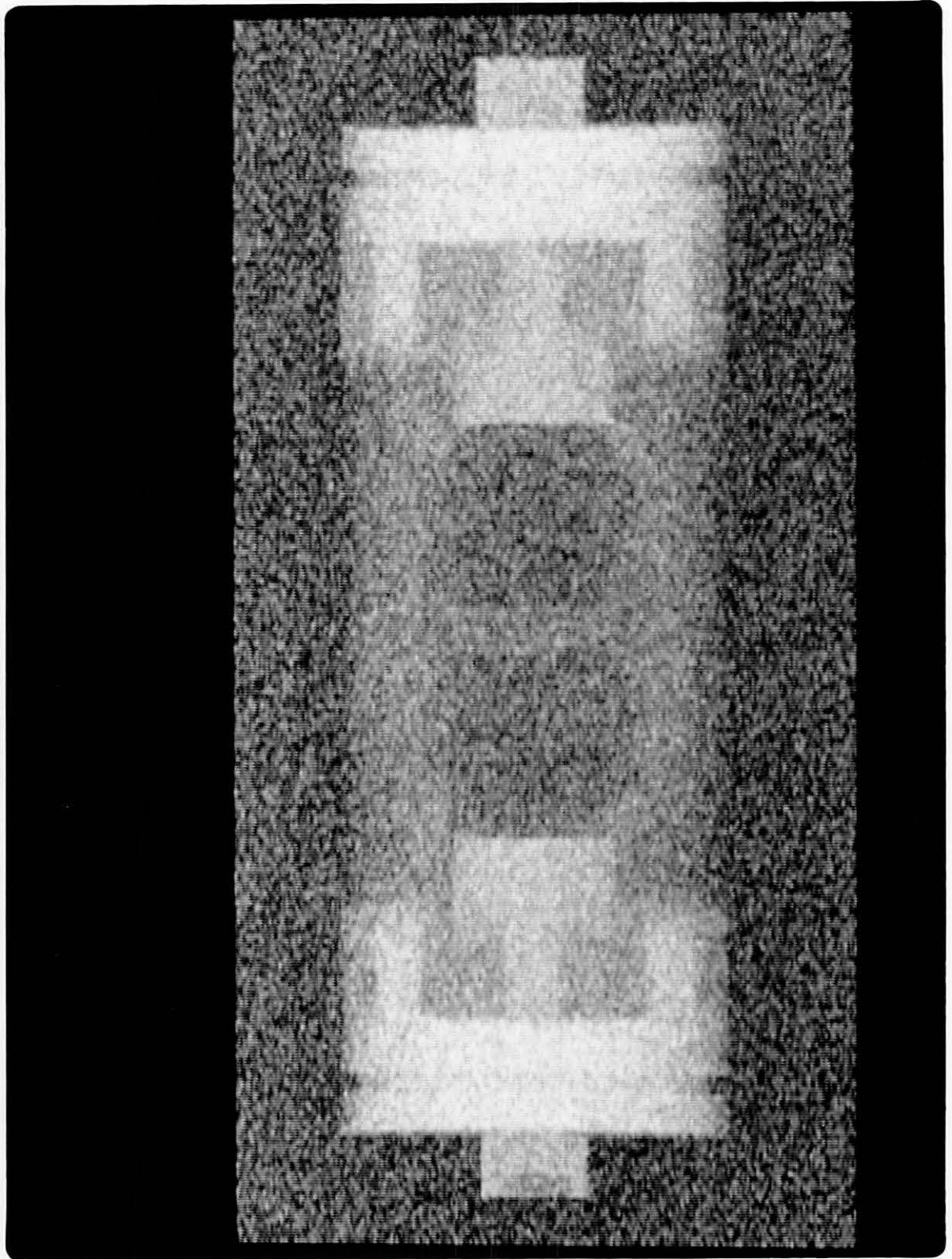


Table 4.1: Result of program run on air-conditioner part

number of neutrons absorbed	2.45(10^5)
number interacted with foil	1.89(10^7)
number neutrons missed foil	1.63(10^5)
number lost in direction opposite foil	6.76(10^5)
total number of thermal neutrons processed	2.00(10^7)

Validation of program results

Due to the low neutron flux and low L/D ratio of the radiography beam port on the Iowa State University UTR-10 reactor, the image quality obtained for an aluminum sample such as that shown in Fig. 4.1 is poor. Although this reactor is far from an ideal facility for neutron radiography, the radiographs produced can be used to make comparisons with the simulation results. Work has been undertaken to validate the results of simulation runs by direct comparison with experimentally measured foil activations from the reactor beam. A sample of simple geometry was used, and the activation on and off the image was compared to the results obtained with the simulation code. The proportion of similarity is a measure of the validity of the model.

A two inch thick brick of lead was placed in the radiography beam. Behind this brick was placed a gold foil. Following irradiation at 10 kW for two hours, the activity of the foil was measured. This activity was used to compute the flux of the beam following passage through the lead brick. This flux was determined to be $6.58(10^6)$ n/cm²/s. The total number of thermal neutrons incident on the lead brick using Eqn. 3.3 was found to be $2.27(10^{13})$.

A simulation run was made for a total of $9.2(10^7)$ thermal neutrons. The flux

after passage through the two inch lead block was calculated to be $5.23(10^6)$ n/cm²/s. This result compares to within 20% of the experimentally measured value. Some of the error in this result could be due to assumptions made within the code. However, it should also be noted that some of the error could be from the experimental measurement of both the flux before and after passage through the lead brick.

Due to the UTR-10 reactor being down for maintenance, the experimental verification of the results of the computer code is not as extensive as desired.

Effects of scattering

The code has been used to study the effects of scattering on simple shapes. For instance, the code was run to see the effects of undercutting. Undercutting is a phenomenon which results when a particle is scattered under an object and thus degrades the image near the edges of this object. Figure 4.3 shows the geometry of the sample. The left portion of this sample is approximately eight mean free paths thick, while the right portion is about four mean free paths thick. The material between the two blocks extends half the depth of the blocks and is one-half mean free paths thick. Since the left block is eight mean free paths thick, most of the neutrons incident in this area will be either absorbed or scattered out of the block. Very few will penetrate the entire thickness and interact with the detector foil. Therefore, the neutrons which interact with the foil under the left block are expected to be mainly the result of scattering from the right block.

The results of this study are shown in Figure 4.4. The curves represent the number of neutrons which hit pixels of the detector foil for two different y values of the pixel array. The upper curve is for a y value where there was material between

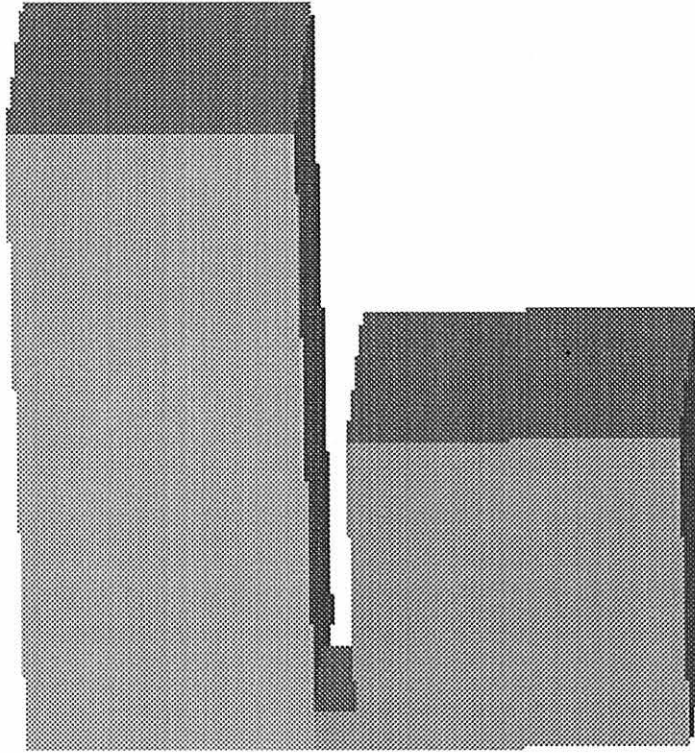


Figure 4.3: Sample geometry used for studying effects of undercutting

the two blocks, while the lower curve is for a y value where the area between the two blocks was void. The material between the two blocks contributed to the scattering under the left block. This resulted in the absolute number of neutrons hitting the pixels for this y value to be greater than the number hitting the pixels for the case in which there was no material between the two blocks. As expected, the amount of undercutting decays exponentially with distance into the left block.

Improving execution time

Improvement in the execution time of the code is one area where work has been performed. In particular, the code has been modified for implementation in parallel

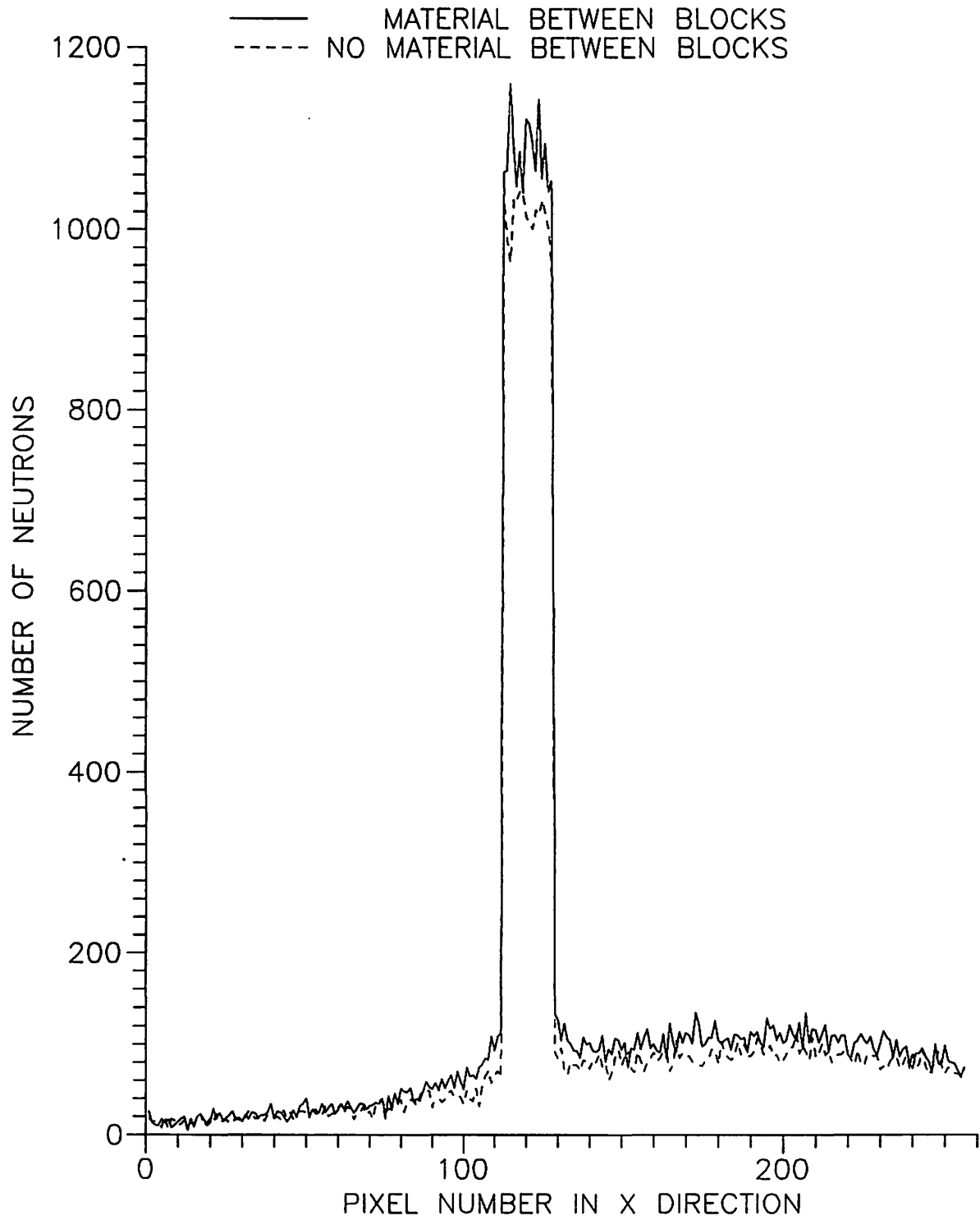


Figure 4.4: Simulation of undercutting by neutrons

environments such as a network of workstations or a Cray or other parallel processing machine. When the code was distributed over a network, the reduction in execution time was found to be a linear function of the number of network nodes used. When a process was distributed over ten workstations, the execution time was approximately one-tenth of the time for the same run on a single workstation [28].

CHAPTER 5. CONCLUSIONS

This code demonstrates a first principles method for treating scattering in complex shapes. A first generation neutron radiography model was developed to emulate the transfer method of neutron radiography. Although this code includes approximations, a solid foundation has been laid, and important modifications will be straight forward to incorporate. Important modifications yet to be completed include the inclusion of the ability to handle flaws and nonhomogeneous materials. It should be pointed out that X-ray scattering can also be treated by the methods developed in this code [7].

Limitations

One of the main objectives of this work is to write a first generation code which incorporates Monte Carlo techniques for the scattering phenomena and utilizes the CAD interface routine available. Since this is a first generation model, there are some limitations to the code which should be discussed. The program assumes that the incident neutrons comprise a parallel beam. So this code would be applicable to simulation of systems which have a high L/D only. Also, there is no compensation made to the image for unsharpness effects due to the thickness of the foil.

Another restriction is the types of materials that can be handled. As the code

now stands, the sample must consist of a homogeneous material. This is because the inclusion of multiple materials would require the use of multiple CAD files which is a feature currently absent from the code.

Also, an important feature the code currently lacks is the ability to handle flaws such as voids or cracks. Incorporation of the ability to handle flaws should be accomplished when the code is modified to allow inclusion of multiple materials. In essence, a flaw model is just another material within the sample geometry.

Since the only modes of interactions allowed are scattering and absorption, this code would probably not be satisfactory for radiography simulation of reactor fuel or other multiplying media. Nondestructive evaluation of radioactive samples is one of the primary uses of neutron radiography. Therefore, it is important for the simulation code to be capable of modeling this NDE technique.

One of the major limitations currently encountered with this code is the time of execution. The reasons for this were addressed in the section on program execution in Chapter 4.

Future Work

Because of the large scope of this work, many items remain which need to be addressed. The results of executions of this code based on a robust Monte Carlo method need to be analyzed. Once the effects from various geometries on the scattering of neutrons are known, a more computationally efficient code can be developed. The scattering effects can be used to establish benchlines for these faster codes.

The results of these studies on scattering of neutrons can be extended to the x-ray simulation code already developed. As it now stands, the x-ray code does

not model photons which scatter. By using the neutron simulation code, the effects on image quality due to scattering can be determined. Then these results can be incorporated into the x-ray code.

Work is under development that will allow for use of multiple material samples. This will most likely be accomplished by using an universal sample file which contains separate geometry sections for each of the different materials. For example, if the object of interest is two plates which have been welded together, there would be three separate geometry components included within the universal file: one for each plate and one for the weld.

The incorporation of flaws can be handled in the same manner as multiple materials. In this case, one of the materials may be a void or an inclusion. The ability to handle multiple materials and flaws will greatly improve the value of this code.

The modeling of the incident neutron beam also has room for improvements. Actual radiography facilities have a wide range of L/D ratios. Therefore, if the divergence of the beam is modeled, the code would be applicable to the various types of nonparallel beams one might encounter. Modeling of the L/D ratio would also improve the match between the simulated image and the actual image. Comparison of simulated and actual images makes the effect of geometric blurring readily evident. This effect needs to be taken into account.

Also, every neutron beam has an unique energy distribution. Modeling of this distribution would allow examination into differences in neutron sources and the beams they produce.

Preliminary investigations into flux studies with the simulation code indicate agreement within 20% of experimental measurements. Improving these results is an

area where further work is warranted. This work could take the form of improvements to the code, and/or better experimental measurements of the fluxes within the radiography beam.

BIBLIOGRAPHY

- [1] Metals Handbook, 9th Edition, Vol 17. Materials Park, Ohio: ASM International, 1989.
- [2] L. E. Bryant and P. McIntire, Ed. Nondestructive Testing Handbook, 2nd Edition, Vol 3. American Society for Nondestructive Testing, 1985.
- [3] H. M. Burte and D. E. Chimenti. "Unified Life Cycle Engineering: An Emerging Design Concept", in Review of Progress in Quantitative Nondestructive Evaluation, Vol 6B, D. O. Thompson and D. E. Chimenti, Ed., New York: Plenum Press, 1987.
- [4] J. N. Gray, T. A. Gray, N. Nakagawa, and R. B. Thompson. "Models for Predicting NDE Reliability" in Metals Handbook, 9th Edition, Vol 17. Materials Park, Ohio: ASM International, 1989.
- [5] R. B. Thompson and T. A. Gray. "A Model Relating Ultrasonic Scattering Measurements Through Liquid-Solid Interfaces to Unbounded Medium Scattering Amplitudes." J. Acoust. Soc. Am., Vol 74, 1983.
- [6] B. A. Auld, F. G. Muennemann, and D. K. Winslow. J. Nondestr. Eval., Vol 2, 1982.
- [7] J. N. Gray. "Three Dimensional Modeling of Projection Radiography," in Review of Progress in Quantitative Nondestructive Evaluation, Vol 7A, D. O. Thompson and D. E. Chimenti, Ed., New York: Plenum Press, 1988.
- [8] W. D. Cowie "Fracture Control Philosophy" in Metals Handbook, 9th Edition, Vol 17. Materials Park, Ohio: ASM International, 1989.
- [9] L. L. Carter and E. D. Cashwell. Particle-Transport Simulation with the Monte Carlo Method. Oak Ridge, Tenn.: Technical Information Center, U.S. ERDA, 1975.

- [10] E. D. Cashwell and C. J. Everett. A Practical Manual on the Monte Carlo Method for Random Walk Problems. New York: Pergamon Press, 1959.
- [11] B. H. Meardon. "A Monte Carlo Computer Program for Neutron Elastic Scattering Simulation." Materials Physics Division, Atomic Energy Research Establishment, Harwell, Berkshire, England, AERE-R.7302, January, 1973.
- [12] J. Spanier and E. M. Gelbard. Monte Carlo Principles and Neutron Transport Problems. Reading, Mass.: Addison-Wesley Publishing Company, Inc., 1969.
- [13] E. D. Cashwell, J. R. Neergaard, W. M. Taylor and G. D. Turner. "MCN: A Neutron Monte Carlo Code." Los Alamos Scientific Laboratory, Los Alamos, N.M., Report LA-4751, 1972.
- [14] L. L. Carter, E. D. Cashwell, C. J. Everett, C. A. Forest, R. G. Schrandt, W. M. Taylor, W. L. Thompson and G. D. Turner. "Monte Carlo Code Development in Los Alamos." Los Alamos Scientific Laboratory, Los Alamos, N.M., Report LA-5903-MS, 1975.
- [15] A. A. Harms and D. R. Wyman. Mathematics and Physics of Neutron Radiography. Dordrecht, Holland: D. Reidel Publishing Company, 1986.
- [16] M. J. Berger. **XCOM: A Computer Code**. Gaithersburg, Md.: National Bureau of Standards, 1987.
- [17] J. R. Lamarsh. Introduction to Nuclear Engineering, 2nd Edn. Reading, Mass.: Addison-Wesley Publishing Company, Inc., 1983.
- [18] E. G. Wiegert. "Design, Parameterization and Use of the Iowa State University UTR-10 for Neutron Radiography." M.S. Thesis, Iowa State University, Ames, Iowa, 1990.
- [19] F. W. Walker, D. G. Miller and F. Fiener. Nuclides and Isotopes. 14th Ed. San Jose, Calif.: General Electric Company, 1989.
- [20] A. Laporte and J. Mars. "Two Examples of Quantitative Neutronography" in Radiography with Neutrons. M. Hawkesworth, Ed., London: The British Nuclear Energy Society, 1975.
- [21] D. Kedem and A. Ariel. "Measurement of the Amount and Distribution of Silicon in Steel using Neutron Radiography" in Radiography with Neutrons. M. Hawkesworth, Ed., London: The British Nuclear Energy Society, 1975.

- [22] P. von der Hardt and H. Röttger, eds. Neutron Radiography Handbook. Dordrecht, Holland: D. Reidel Publishing Company, 1981.
- [23] Structural Dynamics Research Corporation. **I-DEAS**. Milford, Ohio: Structural Dynamics Research Corporation, 1991.
- [24] J. J. Duderstadt and L. J. Hamilton. Nuclear Reactor Analysis. New York: John Wiley & Sons, 1976.
- [25] H. Goldstein. Classical Mechanics. Reading, Mass.: Addison-Wesley Publishing Company, Inc., 1950.
- [26] I. Lux and L. Koblinger. Monte Carlo Particle Transport Methods: Neutron and Photon Calculations. Boca Raton, Fla.: CRC Press, 1991.
- [27] D. J. Hughes and J. A. Harvey. Neutron Cross Sections. Upton, N.Y.: Brookhaven National Laboratory, 1955.
- [28] V. I. Wijaya. "Distributed Computing with C-Linda." M.S. Thesis, Iowa State University, Ames, Iowa, 1993.

APPENDIX A. NEUTRON RADIOGRAPHY TERMINOLOGY

barn unit of area equal to 10^{-24} cm² typically used in the expression of cross-sections

converter metallic foil, usually gadolinium or indium, used to convert non-ionizing neutrons to ionizing radiation (internal conversion electrons, gamma rays, alpha or beta particles) capable of developing radiographic film

cross-section (σ) isotopically dependent probability of a particular neutron interaction with a nuclide usually measured in units of barns per atom

electron volt (eV) unit of energy equal to 1.60219E-19 joules

epithermal neutron neutron whose energy is usually accepted to range from 1 eV to 100 eV

fast neutron neutron whose energy is usually accepted to be greater than 100 eV

isotope components of the same chemical element with different numbers of neutrons

mean free path (λ) the average distance a neutron will travel between interaction sites, the value of λ is equal to the inverse of the total macroscopic cross section for the material of interest

neutron subatomic particle having no charge with a mass of 1.00866491 on the carbon-12 scale

thermal neutron neutron in thermal equilibrium with surrounding atoms and having a most probable energy of 0.0253 eV (2200 m/s)

APPENDIX B. PROGRAM INPUTS

PARAMFILE name of input parameter file ("filename.par")

SIGSCAT thermal microscopic scattering cross-section (barns) of sample

SIGTOT thermal microscopic total cross-section (barns) of sample

MACRO thermal macroscopic total cross-section (1/cm) of sample

ATWT sample atomic weight (based on C-12 = 12.00000)

X1,Y1 start coordinates of detector grid (cm)

X2,Y2 final coordinates of detector grid (cm)

SDIST z location of the source (cm)

NX,NY number of horizontal and vertical detector cells (<257)

CASE flag for neutron (1) or x-ray simulation (2)

CDRATIO cadmium ratio of the incident flux

TE time of target irradiation (s)

OPTION flag for inputting thermal flux(1) or total number of neutrons in beam
(2)

IO incident total neutron flux ($\text{n}/\text{cm}^2/\text{s}$)

DESIRED number of thermal neutrons incident on sample (n)

OUTFILE output file name for rhos ("filename.dat")

SCALE flag for automatic (1) or manual scaling of image (2)

MAXI,MINI maximum and minimum values about which to manually scale image

PROGRESS program status monitoring file name ("filename.sts")

HOWOFTEN integer signifying how often user wants the status file updated (i.e., an entry of "1.D6" means user wants the status updated every time one million neutrons have been processed)

NEUTARR output file name for number of neutrons in each pixel of detector ("filename.arr")

OUTFILEA image output file name ("filename.ima")

FOILTH thickness of the indium transfer foil (cm)

TW time expired between end of foil irradiation and placement of foil in contact with film (s)

TC time foil was in contact with film (s)

UNVFILE CAD input filename ("filename.unv")

THICKFILE output filename for sample thicknesses ("filename.tck")

GEN flag for generation of new *.tck file (1) or reading of existing file (2)

BX1,BY1 start coordinates of the beam (cm)

BX2,BY2 end coordinates of the beam (cm)

IFLAG seed for random number generator

CRASH flag for new run (0) or restart of crashed run (1)

OLDARR file containing various parameter which are read in during restart of crashed run ("filename.arr")